Published in final edited form as:

Nat Cell Biol. 2020 April ; 22(4): 412–424. doi:10.1038/s41556-020-0481-4.

Copper is an essential regulator of the autophagic kinases ULK1/2 to drive lung adenocarcinoma

Tiffany Tsang[1,2,4], **Jessica M. Posimo**[1,4], **Andrea A. Gudiel**[1], **Michelle Cicchini**[1], **David M. Feldser**[1,3], **Donita C. Brady**[1,3,*]

[1]Department of Cancer Biology, Perelman School of Medicine, University of Pennsylvania, Philadelphia, PA, 19104, USA.

[2]Cell and Molecular Biology Graduate Group, University of Pennsylvania, Philadelphia, PA, 19104, USA.

[3]Abramson Family Cancer Research Institute, Perelman School of Medicine, University of Pennsylvania, Philadelphia, PA, 19104, USA.

Abstract

While the transition metal copper (Cu) is an essential nutrient that is conventionally viewed as a static cofactor within enzyme active sites, a nontraditional role for Cu as a modulator of kinase signaling is emerging. We discovered that Cu is required for the activity of the autophagic kinases ULK1/2 through a direct Cu-ULK1/2 interaction. Genetic loss of the Cu transporter *Ctr1* or mutations in ULK1 that disrupt Cu-binding reduced ULK1/2-dependent signaling and autophagosome complex formation. Elevated intracellular Cu levels are associated with starvation induced autophagy and sufficient to enhance ULK1 kinase activity and in turn autophagic flux. The growth and survival of lung tumors driven by $KRAS^{G12D}$ is diminished in the absence of *Ctr1*, depends on ULK1 Cu-binding, and is associated with reduced autophagy levels and signaling. These findings suggest a molecular basis for exploiting Cu-chelation therapy to forestall autophagy signaling to limit proliferation and survival in cancer.

[*]**Corresponding author.** Correspondence and requests for materials should be addressed to Donita C. Brady (bradyd@pennmedicine.upenn.edu).

Author contributions. T.T. and J.M.P contributed equally to this work. T.T. contributed to the study design, generated cell lines and plasmids, prepared samples for ICP-MS, performed Western blot analysis, immunocomplex kinase assays, crystal violet growth assays, co-immunoprecipitations, qPCR, and *in vivo* xenograft mouse work, analyzed data, and prepared figures. J.M.P. generated cell lines, performed flow cytometry, immunofluorescence imaging, live cell imaging, immunohistochemical analysis, Western blot analysis, crystal violet growth assays, quantitative PCR (qPCR), and assisted in *in vivo* $KRAS^{G12D}$ mouse tumor model work. A.A.G. maintained *in vivo* $KRAS^{G12D}$ mouse tumor models and performed *in vivo* $KRAS^{G12D}$ mouse tumor model imaging. M.C. generated tumors *in vivo* $KRAS^{G12D}$ mouse model. D.M.F. contributed to the study design, provided expertise *in vivo* mouse tumor models, and facilitated data analysis. D.C.B conceived of the project, contributed to the study design, generated cell lines, plasmids, and recombinant proteins, performed Cu-binding assays, *in vitro* kinase assays, immunofluorescence imaging, and *in vivo* xenograft mouse work, analyzed data, prepared figures, and wrote the manuscript. All authors read and provided feedback on manuscript and figures.

[4]These authors contributed equally to this work.

Competing interests. D.C.B holds ownership in Merlon Inc. D.C.B. is an inventor on the patent application 20150017261 entitled "Methods of treating and preventing cancer by disrupting the binding of copper in the MAP kinase pathway". No potential conflicts of interest were disclosed by the other authors.

Introduction

By default, the dynamic and adaptive nature of signaling networks allows them to respond and, in some cases, sense extracellular and intracellular inputs[1]. While growth factors, nutrients, and metabolites are well-appreciated regulators of cell proliferation, the contribution of transition metals to cellular processes that support proliferation and contribute to malignant transformation are understudied. The transition metal copper (Cu) is essential for a diverse array of biological processes from cellular proliferation, neuropeptide processing, free radical detoxification, and pigmentation[2]. The importance of intact Cu homeostatic mechanisms for cell growth control is underscored by the stunted growth and failure to thrive associated with Cu deficiency in Menkes disease patients[3] and the increased prevalence of cancer in patients and animal models with hereditary Cu overload in Wilson disease[4–6]. However, the dysregulated growth phenotypes associated with alterations in Cu availability cannot be fully explained by the limited number of Cu-dependent enzymes that traditionally harness the redox potential of Cu as a structural or catalytic cofactor.

Several recent studies have illuminated functions for Cu as a non-structural intracellular mediator of signaling by directly connecting Cu to signaling pathway components that modulate cell proliferation or lipid metabolism[7–9]. We previously showed that in response to growth factors, Cu contributes to the amplitude of canonical MAPK signaling through an interaction between Cu and the kinases MEK1 and MEK2[7]. Examination of this signaling mechanism in the context of cancer revealed that $BRAF^{V600E}$-driven tumors depend on MEK1/2 association with Cu, and moreover, are sensitive to Cu-chelating drugs[8,10,11]. In Wilson disease, Cu influences 3',5'-cyclic AMP (cAMP)-mediated lipolysis downstream of β-adrenergic receptor signaling by directly inhibiting the phosphodiesterase PDE3B[9], serving as one molecular mechanism to explain the connection between aberrant Cu accumulation and altered lipid metabolism[5]. These findings bolster a paradigm linking Cu levels to signaling pathway components that are essential for normal physiology, but that become dysregulated in multiple disease states including cancer. Thus, uncovering additional kinases that are regulated by Cu levels is needed to further define Cu-dependent cellular processes that may contribute to the efficacy of Cu chelators for cancer therapy[12].

Results

Cu binds to ULK1 and ULK2 and is required for kinase activity.

To explore other Cu-dependent kinases, we first performed an alignment of the Cu-binding sequence in MEK1[8] against kinase domains and identified the autophagy regulatory kinases ULK1 and ULK2 as sharing significant sequence similarity at the amino acids (H188, M230, and H239) required for Cu-binding in MEK1 (Fig. 1a). Both ULK1 and ULK2 bind to a Cu-charged resin, but not a metal free resin control, Fe-, or Zn-charged resin (Fig. 1b,c). To investigate the impact of Cu-binding to ULK1 and ULK2 function, we first tested whether Cu is directly required for ULK1 and ULK2 kinase activity. ULK1 and ULK2 *in vitro* kinase activity was enhanced in response to increasing concentrations of $CuCl_2$ (Fig. 1d,e and Extended Data Fig. 1a,b) and inhibited when treated with increasing concentrations of the Cu chelator tetrathiomolybdate (TTM) (Fig. 1f,g and Extended Data Fig. 1c,d). The

reduced ULK1 and ULK2 kinase activity in presence of TTM was similar to inhibition achieved with the ULK1/2 inhibitor MRT68921[13] (Fig. 1f,g and Extended Data Fig. 1c,d).

Reducing or increasing intracellular Cu levels modulates ULK1/2 kinase activity.

ULK1/2 are well-established downstream targets of the protein kinase mammalian target of rapamycin (mTOR)[14–17]. When associated with rapamycin-sensitive mTOR complex 1 (mTORC1)[18], mTOR controls cellular energetics by driving anabolic processes, such as lipid, nucleotide, and protein synthesis[19], and suppressing catabolic processes[14–17], like autophagy. mTOR kinase activity is blocked in response to amino acid deprivation[20–22], low cellular ATP levels[23,24], or rapamycin treatment[25,26]. This in turn relieves the inhibitory phosphorylation of ULK1 and ULK2 and initiates the formation of an autophagosome[14–17], which degrades and recycles proteins, lipids, and organelles to restore nutrient balance in the form of building blocks for metabolic pathways. To investigate the relationship between Cu and mTORC1-ULK1/2 signaling in mammalian cells, Cu-replete and Cu-deficient cells were generated by expressing the high affinity Cu transporter CTR1 (WT) or an empty vector (VO) in immortalized *Ctr1*$^{-/-}$ mouse embryonic fibroblasts (MEFs). Intracellular Cu levels in CTR1^{WT} expressing *Ctr1*-null MEFs are comparable to *Ctr1*$^{+/+}$ MEFs as confirmed by reduced CCS protein stability[27], which is degraded in a Cu-dependent fashion, increased Cu levels via inductively coupled plasma mass spectrometry (ICP-MS), and elevated fluorescence from the CF4 probe[28], which detects labile Cu (Fig. 1d and Extended Data Fig. 1e–h). *Ctr1* loss reduced ULK1-mediated phosphorylation of ATG13 under basal conditions and the elevated phosphorylation of ATG13 that occurs upon amino acid deprivation[14–17] was only observed in the Cu-replete conditions (Fig. 1h and Extended Data Fig. 1i). In contrast, PI3K/AKT signaling-mediated phosphorylation[29] of mTOR^{S2448} and mTOR phosphorylation[30–32] of ULK1^{S757}, p70S6K^{T389}, and mTOR^{S2481} remained unchanged upon reduced Cu levels (Fig. 1h). These data suggest that Cu is required for ULK1 activity but not its upstream regulation by mTORC1 or mTOR itself. In agreement, ULK1 kinase activity is elevated upon amino acid withdrawal in Cu-replete cells but is blunted in the Cu-deficient cells (Fig. 1i and Extended Data Fig. 1j). Additionally, MEFs lacking the Cu exporter *Atp7a*, which have elevated intracellular Cu levels, also had increased ULK1 kinase activity (Fig. 1j and Extended Data Fig. 1k). These findings that reduced Cu levels decrease ULK1/2-dependent signaling downstream of mTORC1 inhibition (Fig. 1h–j) suggest that autophagy was a yet to be identified Cu-dependent process.

Cu is both necessary and sufficient for autophagic flux in an ULK1/2-dependent fashion.

The ULK1-ATG13 complex senses low-energy and nutrient depleted cellular states and initiates autophagosome formation[14–17]. To determine whether changes in levels of Cu affect ULK1/2-dependent autophagy, Cu-replete or Cu-deficient MEFs were exposed to amino acid deprivation[20–22] or rapamycin[25,26], which inhibit mTOR. Specifically, autophagic flux was measured by three techniques, including *i*) Western blot analysis of the processing of LC3 from its cleaved form (LC3-I) to phosphatidylethanolamine-conjugated form (LC3-II)[33], *ii*) flow cytometry measurement of the ratio of autolysosomes (mCherry-LC3B) to autophagosomes (EGFP-LC3B)[34], and *iii)* immunofluorescence detection of the abundance of autophagosomes (mCherry-EGFP-LC3 positive puncta) and autolysosomes (mCherry-LC3 positive puncta)[35]. These studies revealed that loss of *Ctr1* significantly reduced LC3-I

processing (Fig. 2a and Extended Data Fig. 2a) and prevented autophagosome to autolysosome conversion upon autophagy induction (Fig. 2b–d). Further, under basal conditions the number of mCherry-EGFP-LC3 positive puncta was significantly reduced, indicating a potential block in autophagosome formation and in turn recruitment of LC3B (Fig. 2c,d). In contrast, CRISPR/Cas9-mediated knockdown of endogenous *Atp7a* (Extended Data Fig. 2b) caused elevated Cu levels that were sufficient to enhance LC3-II levels (Fig. 2e and Extended Data Fig. 2c) and autophagic flux (Fig. 2f–h). Collectively, these data suggest that the levels of Cu could serve as a rheostat for ULK1/2-dependent autophagy by regulating ULK1/2 kinase activity in an mTOR-dependent fashion.

Since altering Cu levels has been shown to affect MAPK signaling[7,8], we interrogated the contribution of the MAPK pathway to Cu-mediated regulation of autophagy via genetic and pharmacologic approaches. First, we directly tested whether disrupting MEK1 Cu-binding was sufficient to reduce autophagy in the presence (*Ctr1*$^{flox/flox}$) or absence (*Ctr1*$^{-/-}$) of Cu transport. While expression of ***C***u-***b***inding ***m***utant (CBM) of MEK1[8] reduced phosphorylation of ERK1/2 (Extended Data Fig. 2d), LC3-II levels were unchanged and Cu-dependent autophagic flux was still observed in *Ctr1*$^{-/-}$ MEFs (Extended Data Fig. 2e,f). Second, treatment with the MEK1/2 inhibitor, trametinib, which abolished phosphorylation of ERK1/2, did not phenocopy the reduced autophagic flux in the absence of *Ctr1* (Extended Data Fig. 2g,h). Consistent with these findings, expression of a gain-of-function (GOF) ERK2 mutant[8], which bypasses the ability of Cu to influence MEK1/2 activity in *Ctr1*$^{-/-}$ MEFs (Extended Data Fig. 2i), did not increase LC3-II levels in cells devoid of significant Cu transport (Extended Data Fig. 2j,k). Finally, while increasing Cu levels via *Atp7a* knockdown is sufficient to increase phosphorylation of ERK1/2 (Fig. 2e), loss of *Atp7a* in MEFs lacking the key autophagy regulator *Atg5* (Extended Data Fig. 2b), which is part of the ubiquitin-like conjugation system that lipidates LC3[33], failed to re-establish autophagy (Extended Data Fig. 2l). Collectively, these data indicate that Cu-dependent autophagy is mechanistically independent of Cu-regulated MEK1/2 activity and upstream of ATG5, which is required for autophagosome nucleation.

Elevated intracellular Cu levels are associated with starvation induced autophagy and are required for autophagosome complex formation.

Since our findings suggest that Cu is required for ULK1/2-dependent signaling and autophagic flux in response to mTOR inhibition, we next hypothesized that Cu levels may fluctuate in an acute manner after autophagy induction. Interestingly, a statistically significant elevation in labile intracellular Cu levels, as measured by increased fluorescence of the Cu probe CF4[28] and not its control (Ctrl-CF4)[28], was detected in a time-dependent fashion post amino acid withdrawal (Fig. 3a,b, Extended Data Fig. 3a,b, and Supplementary Video 1–4). Thus, the requirement for Cu for efficient autophagic flux is driven by Cu fluctuations that support ULK1/2 kinase activity. While ULK1/2 activation is typically a prerequisite for LC3 processing by the ubiquitin-like conjugation system on the forming autophagosome[14], several upstream ULK1/2-dependent molecular events are essential to initiate autophagosome formation[36,37] (Extended Data Fig. 3c). Specifically, active ULK1 translocates to the ER with its constitutive binding partners ATG13 and FIP200 to drive phagophore formation by phosphorylating core components of the class III PI3K VPS34

complex, which includes BECLIN-1, PIK3R4 (p150), and VPS34 itself[14–17,38–40]. The ULK1-mediated phosphorylation of BECLIN-1 or ATG14 within VPS34 complex 1 stimulates VPS34 activity, which converts phosphatidylinositol to PI3P[40,41]. The generation of PI3P serves as a docking site for FYVE domain containing proteins, like DFCP1 and WIPI1, that recruit the ubiquitin like conjugation complex ATG5-ATG12-ATG16 to lipidate LC3B[36,42]. To dissect the contribution of Cu to the molecular events directly downstream of ULK1-dependent autophagosome formation, we visualized ULK1 complex translocation to puncta, (EGFP-ATG13 or EGFP-FIP200), VPS34 complex PI3P generation on puncta (EGFP-DFCP1), and PI3P effector translocation to puncta (EGFP-WIPI1) in response to amino acid deprivation in the presence (*Ctr1*$^{flox/flox}$) or absence (*Ctr1*$^{-/-}$) of Cu transport. Cu deficiency significantly decreased both ATG13, FIP200, WIPI1, and DFCP1 puncta formation in response to amino acid deprivation, indicating that Cu transport contributes to the early steps of phagophore nucleation (Fig. 3c–j). Defective recruitment of these initiating complexes and PI3P production, limited the number of EGFP-LC3 positive autophagosomes measured by flow cytometry[43] (Fig. 3k and Extended Data Fig. 3d), an effect that was rescued by loss of the Cu exporter *Atp7A* (Fig. 3l). A selective requirement for Cu in the regulation of autophagosome formation was observed, as the Cu chelator TTM reduced EGFP-LC3 positive autophagosome number, while the iron (Fe) chelator desferoxamine (DFO) had no effect (Extended Data Fig. 3e,f). These findings suggest that ULK1/2-driven autophagy initiation requires Cu transport.

Genetic ablation of *Ctr1* decreases autophagy and proliferation to reduce tumorigenesis and sensitizes cancer cells to starvation in a mouse model of *Kras*^{G12D}-driven lung cancer.

Increased levels of basal autophagy in some cancers represents a vulnerability to autophagy inhibition[44]. We previously demonstrated that genetic ablation of *Ctr1* reduced BRAF^{V600E}-driven lung tumor development, leading to a survival advantage[8]. While the reliance of BRAF^{V600E}-driven tumors on both autophagy[45] and Cu transport[8] could be exploited therapeutically, activating mutations in *KRAS* are the most common driver event in this disease[46]. Importantly, oncogenic *Kras*^{G12D}-driven lung adenocarcinomas also depend on efficient autophagy for tumor maintenance[47]. Deletion of the critical autophagy component *Atg7* converts *Kras*^{G12D}-driven adenomas and adenocarcinomas to oncocytomas, a benign tumor type characterized by an accumulation of dysfunctional mitochondria[47]. To investigate the relationship between Cu, oncogenic KRAS-driven lung cancer, and autophagy, we investigated whether loss of *Ctr1* disrupts autophagy in an autochthonously arising KRAS^{G12D}-driven lung adenocarcinoma model. We transduced cohorts of *LSL-**K**ras*$^{G12D/+}$;*Tr**p**53*$^{flox/flox}$;*Rosa26::LSL-**Luc*** (KPLuc) mice via intratracheal administration of lentivirus expressing Cre recombinase, Cas9, and sgRNA targeting either *β-GAL* or *Ctr1*. Tumor growth was monitored over time with luminescence imaging. Strikingly, we found that genetic targeting of Cu transport blunts the development of KRAS^{G12D}-driven lung tumors (Fig. 4a,b,d,g and Extended Data Fig. 4a–c). Tumor volume at 16 weeks was significantly decreased in mice with CRISPR-mediated deletion of *Ctr1* (Fig. 4a,b,g). *Ctr1* loss was confirmed by increased CCS levels in the tumor tissue (Fig. 4c,e,h) and correlated with reduced *in vivo* tumor cell proliferation (Ki67-positive staining, Fig. 4f,i). Molecularly, the established *Ctr1* deficient KPLuc tumors had decreased LC3-positive staining, increased p62-positive staining, and reduced autophagosome number, indicative of diminished

autophagy (Fig. 5a–f). Thus, the loss of *Ctr1* mitigates $KRAS^{G12D}$-mediated autophagy that is necessary for lung tumor growth.

Interestingly, several recent studies reported that genetic disruption of oncogenic KRAS or MAPK pathway inhibition elicits protective autophagy via an ULK1-dependent signaling mechanism and indicate that dual targeting of the canonical MAPK pathway and autophagy may be necessary for anti-tumorigenic activity in KRAS-driven tumors[48–50]. In agreement with our findings that Cu is necessary for MEK1/2[8] and ULK1/2 kinase activity (Fig. 1d–g and Extended Data Fig. 1a–d), loss of *Ctr1* in $KRAS^{G12D}$ lung tumors diminished ERK1/2 activation (Extended Data Fig. 5a,b), while also blunting compensatory autophagy induction via ULK1/2 (Fig. 5a–f). These data suggest that the dual inhibition of these kinase signaling nodes contributes to the reduced *in vivo* tumor cell proliferation (Ki67-positive staining, Fig. 4f,i) associated with *Ctr1* deficiency. However, these results failed to address the extent to which Cu-regulated MAPK signaling versus Cu-mediated autophagy contributes to lung tumor cell growth and survival during $KRAS^{G12D}$-driven tumorigenesis. To begin to interrogate whether the requirement for Cu to induce autophagy is necessary for oncogenic $KRAS^{G12D}$ lung tumor cell phenotypes, we established lung adenocarcinoma cell lines isolated from *LSL-**K**ras*$^{G12D/+}$;*Tr**p**53*$^{flox/flox}$ (KP) mice in which *Ctr1* was inactivated via CRISPR/Cas9 (Extended Data Fig. 5c). Targeted disruption of *Ctr1* reduced LC3-II levels in two KP lung adenocarcinoma cell lines as compared to cells transduced with a non-targeting control sgRNA (Fig. 5g and Extended Data Fig. 5d). The dependency of KRAS-driven cancer cell lines on autophagy for growth and survival has been previously evaluated *in vitro* with clonogenic survival assays (Fig. 5h), in which cancer cells are plated in normal media, subsequently starved of amino acids for one day to induce autophagy, and then recovered in normal media for three days, and the ability of the cancer cells to survive is assessed[51]. In agreement with Guo *et* al.[51], CRISPR/Cas9 knockout of *Atg5* in KP lung adenocarcinoma cells significantly reduced the clonogenic survival of cells post starvation, an effect that was phenocopied by *Ctr1* deletion (Fig. 5i,j). Importantly, expression of $ERK2^{GOF}$ was not sufficient to rescue the decrease in clonogenic survival in the absence *Atg5* or *Ctr1* (Extended Data Fig. 5e,f), which suggests that the survival of these lung cancer cells depends on autophagy in a MAPK-independent fashion. Nevertheless, our collective results demonstrate that the dependence of $KRAS^{G12D}$-driven tumors on MAPK signaling and autophagy events can be inhibited by altering Cu levels, which could be achieved with Cu chelators alone.

Binding of Cu to ULK1 is required for autophagy signaling and induction.

To mechanistically interrogate the contribution of Cu-binding to ULK1 signal transduction and autophagy initiation, we next mutated H136, M188, and H197 to alanine, which share conserved primary sequence with the ***C***u-***b***inding ***m***utant (CBM) of MEK1[8] (Fig. 1a). Compared to wild-type ULK1, the $ULK1^{CBM}$ had reduced *in vitro* ability to bind a Cu-charged resin and phosphorylate ATG13 (Fig. 6a,b). While the lack of ULK^{CBM} *in vitro* kinase activity could suggest a Cu-binding independent finding, we previously demonstrated that introduction of mutations at these conserved residues in MEK5, which is highly similar to MEK1/2 and does not bind Cu, did not alter MEK5 kinase activity[8]. Along these lines, the $ULK1^{CBM}$ immunoprecipitated from *Ulk1/2*$^{-/-}$ MEFs deprived of amino acids failed to

phosphorylate ATG13 as compared to the exogenous ULK1^{WT} (Fig. 6c). While both ULK1^{WT} and ULK1^{CBM} were efficiently phosphorylated by AMPK at serine 555 and mTORC1 at serine 757 when stably expressed in *Ulk1/2*$^{-/-}$ MEFs (Extended Data Fig. 6a), the ULK1^{CBM} exhibited a mobility shift that corresponded to reduced ULK1 autophosphorylation due to defective kinase activity (Extended Data Fig. 6b). Further, despite decreased kinase activity the ULK1^{CBM} retained strong interactions with canonical binding partners ATG13, ATG101, and FIP200, suggesting that the three-dimensional structure of ULK1 is not destabilized upon introduction of mutations into ULK1^{CBM} (Extended Data Fig. 6c). To evaluate the consequence of disrupting ULK1 Cu-binding on autophagic flux, signaling, and autophagosome formation, *Ulk1* and *Ulk2* knockout MEFs were generated via CRISPR/Cas9 and validated to have reduced autophagic flux in response to amino acid deprivation, but as previously reported still retain visible levels of LC3-II[52] (Extended Data Fig. 6d–f). Only expression of ULK1^{WT} partially rescued LC3-II levels, phosphorylation of ATG13, and autophagosome formation in the context of *Ulk1/2* deficiency, indicating that Cu binding is required to restore autophagy downstream of ULK1 (Fig. 6d,e, Fig. 7a–f, and Extended Data Fig. 6g,h). Finally, consistent with Cu-dependent autophagy acting solely through ULK1/2, we found that loss of *Ctr1* in MEFs deficient in *Ulk1/2* does not further alter autophagic flux (Fig. 6f and Extended Data Fig. 6i), as measured by LC3-II levels. This further bolsters the conclusion that Cu levels mechanistically contribute to autophagy via ULK1/2 and not another Cu-dependent parallel pathway.

Binding of Cu to ULK1 is required for KRAS^{G12D}-driven tumor growth and cancer cell survival in response to starvation.

To translate our finding that Cu-binding to ULK1 is required for autophagy to KRAS-driven tumorigenesis, we next tested and found that blocking ULK1 Cu-binding was associated with reduced tumor growth kinetics and endpoint tumor weight of KRAS^{G12D}-transformed *Ulk1*$^{-/-}$ immortalized MEFs stably expressing the ULK1^{CBM} compared to ULK1^{WT} (Extended Data Fig. 7a–c). To investigate whether these results could be extrapolated to the setting of endogenous oncogenic KRAS tumorigenesis, *Ulk1* and *Ulk2* were knocked out by CRISPR/Cas9 in mouse *KRAS* mutant lung adenocarcinoma cell lines (Extended Data Fig. 7d). As expected, loss of endogenous *Ulk1/2* decreased the levels of LC3-II and phosphorylation of ATG13 (Fig. 8a,b and Extended Data Fig. 7e,f). Targeted disruption of *Ulk1/2* reduced *in vivo* tumor growth to a similar extent to loss of *Atg5* (Fig. 8c–e). In agreement with Cu being required for ULK1 kinase activity, only ULK1^{WT}, but not ULK1^{CBM} could partially restore autophagic flux, signaling, and efficient subcutaneous tumor growth (Fig. 8a–e). Given that Cu mechanistically contributes to autophagy via ULK1/2, the clonogenic survival of KP adenocarcinoma cells was dependent on ULK1/2 but was not further exacerbated by deletion of *Ctr1* (Fig. 8f,g and Extended Data Fig. 7g). Together, these data support a mechanism to regulate ULK1 activity via Cu binding to promote nutrient deprived or oncogene-driven autophagy that is required for tumorigenesis.

Discussion

Despite evidence that Cu homeostasis is essential for life[2], relatively little is known about cellular pathways that respond directly to Cu levels. We show here that Cu directly modulates the activity of the autophagic kinases ULK1 and ULK2 to function as an endogenous rheostat to control autophagy during nutrient deprivation. These findings highlight a molecular basis for a Cu-dependent cellular process to support energy homeostasis. One enticing hypothesis is that sensing Cu abundance through dynamic signaling networks may help cells adapt to environmental changes that would require differential cellular metabolism. By extension, limiting Cu availability or decreasing the binding of Cu to ULK1 may be an attractive therapeutic opportunity to reduce the growth of oncogene-driven lung adenocarcinomas that in part rely on autophagy for tumor maintenance and cell survival. Interestingly, models of KRAS-driven lung cancer have differing levels of autophagy dependence based on which tumor suppressor is dysregulated, suggesting that the utility of reducing Cu levels to dually target autophagy and MAPK signaling could be exploited more broadly. Further, while targeting protein kinase catalytic activity is a proven approach in the landscape of cancer therapeutics, orthogonal approaches that exploit the Cu-dependency of kinases that are critical for maintaining cellular processes essential for tumor growth, such as autophagy, represents an untapped therapeutic opportunity.

Extended Data

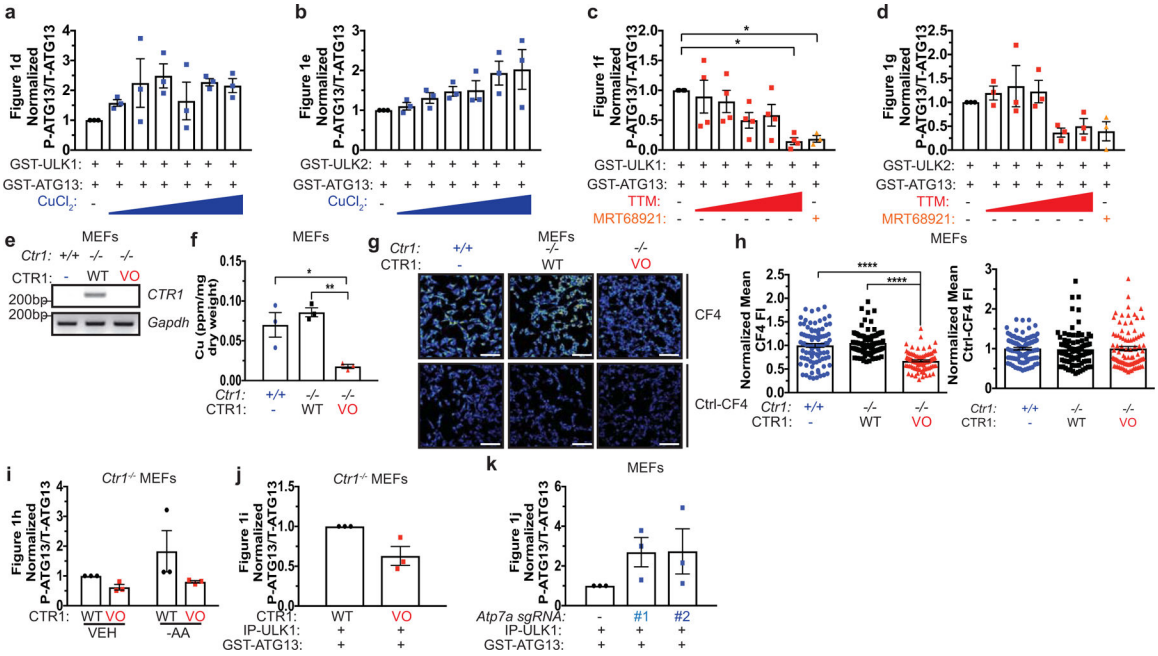

Extended Data 1. Cu is both necessary and sufficient for ULK1 and ULK2 kinase activity.

a,b,c,d, Scatter dot plot with bar at mean normalized ΔPhosphorylated (P)-ATG13/Total (T)-ATG13 from Figure 1d,e,g. n=3 biologically independent experiments, Figure 1d,e,g, or n=4 biologically independent experiments, Figure 1f. Results were compared using a one-way ANOVA followed by a Tukey's multi-comparisons test. 0 vs. 50 μM TTM, *, P=0.0151; 0

vs. 10 μM MRT68921, *, P=0.0395. **e**, RT-PCR detection of indicated mRNAs from *Ctr1*$^{+/+}$ MEFs or *Ctr1*$^{-/-}$ MEFs stably expressing *CTR1*^{WT} (WT) or *empty vector* (VO). n=1 biologically independent sample. **f**, Scatter dot plot of inductively coupled plasma mass spectrometry (ICP-MS) detection with bar at mean Cu (parts per million, ppm) from *Ctr1*$^{+/+}$ MEFs (+/+) or *Ctr1*$^{-/-}$ MEFs stably expressing WT or VO per sample weight ± s.e.m. n=3 biologically independent samples. Results were compared using a one-way ANOVA followed by a Tukey's multi-comparisons test. *, P=0.05 0.0202; **, P=0.0059. **g**, Representative live cell imaging of the Cu probe CF4 or control Cu probe Ctrl-CF4 from *Ctr1*$^{+/+}$ MEFs (+/+) or *Ctr1*$^{-/-}$ MEFs stably expressing WT or VO. Scale bar, 100 μm. **h**, Scatter dot plot with bar at mean CF4 or Ctrl-CF4 fluorescence intensity (FI) ± s.e.m. from *Ctr1*$^{+/+}$ MEFs (+/+) or *Ctr1*$^{-/-}$ MEFs stably expressing WT or VO. n=90 individual cells. Results were compared using a one-way ANOVA followed by a Tukey's multi-comparisons test. ****, P<0.0001. **i,j,k,** Scatter dot plot with bar at mean normalized ΔP-ATG13/T-ATG13 from Figure 1h,i,j. n=3 biologically independent experiments. Results were compared using a one-way ANOVA followed by a Tukey's multi-comparisons test, an unpaired, two-tailed Student's t-test, or two-way ANOVA followed by a Sidak's multi-comparisons test. ns.

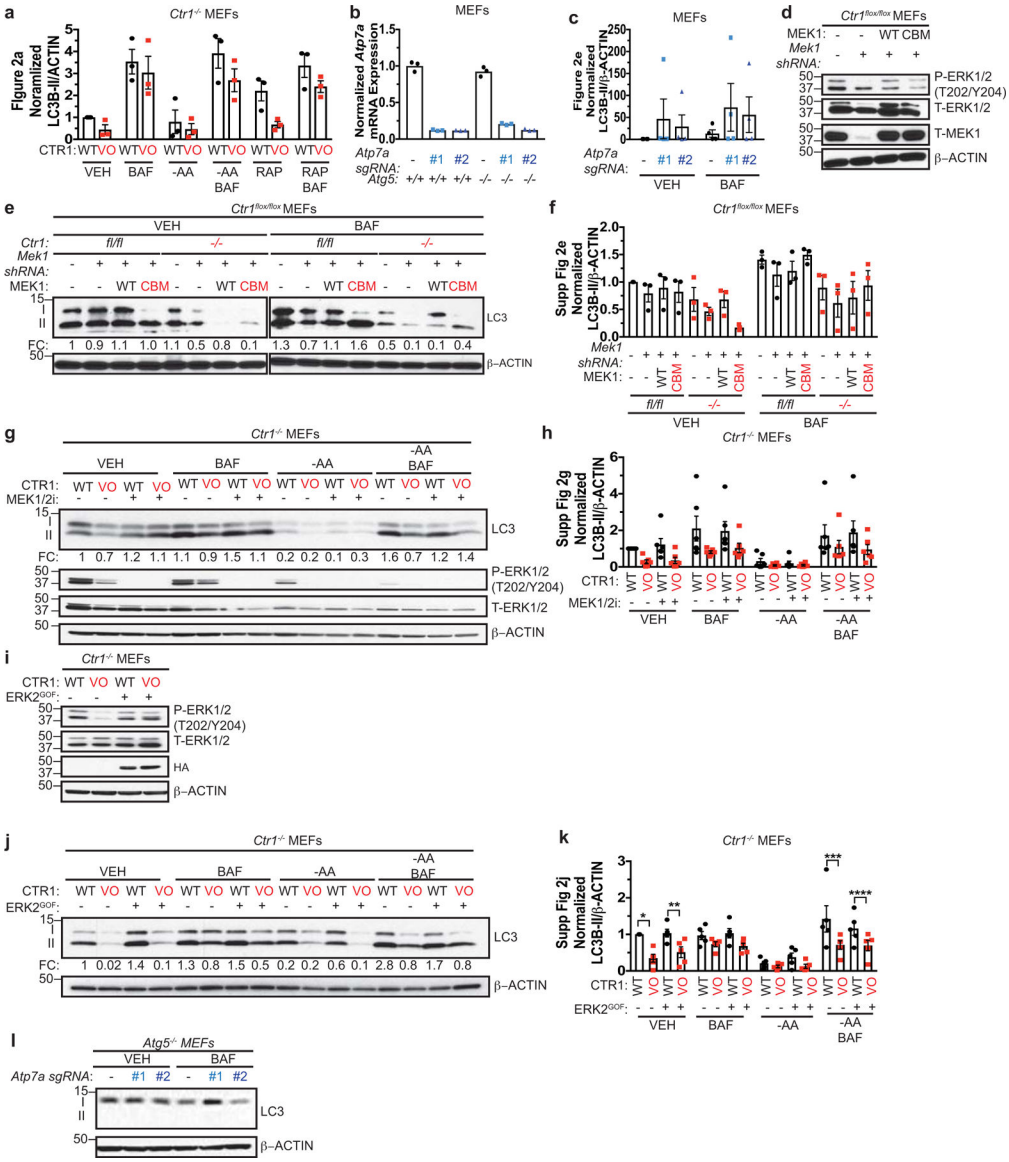

Extended Data 2. Copper is both necessary and sufficient for autophagy induction and signaling in a MAPK signaling independent fashion, upstream of ATG5.

a, Scatter dot plot with bar at mean normalized ΔLC3-II/β-ACTIN from Figure 2a. n=3 biologically independent experiments. Results were compared using a two-way ANOVA followed by a Sidak's multi-comparisons test. ns. **b**, Scatter dot plot with bar at mean normalized expression of *Atp7a* mRNA from MEFs n=1 biologically independent experiment performed in technical triplicate. **c**, Scatter dot plot with bar at mean normalized ΔLC3-II/β-ACTIN from Figure 2e. n=4 biologically independent experiments. Results were compared using a two-way ANOVA followed by a Sidak's multi-comparisons test. ns. **d**, Immunoblot detection of proteins from MEFs. **e**, Immunoblot detection of proteins from treated MEFs. Quantification: ΔLC3-II/β-ACTIN normalized to *fl/fl*, empty vector (−), VEH control. **f**, Scatter dot plot with bar at mean normalized ΔLC3-II/β-ACTIN from Extended Data 2e. n=3 biologically independent experiments. Results were compared using a two-way ANOVA followed by a Tukey's multi-comparisons test. ns. **g**, Immunoblot detection of

proteins from treated MEFs. Quantification: ΔLC3-II/β-ACTIN normalized to WT, VEH control. **h**, Scatter dot plot with bar at mean normalized ΔLC3-II/β-ACTIN from Extended Data 2g. n=6 biologically independent experiments. Results were compared using a two-way ANOVA followed by a Tukey's multi-comparisons test. ns. **i**, Immunoblot detection of proteins from MEFs. **j**, Immunoblot detection of proteins from treated MEFs. Quantification: ΔLC3-II/β-ACTIN normalized to WT, VEH control. **k**, Scatter dot plot with bar at mean normalized ΔLC3-II/β-ACTIN from Extended Data 2j. n=5 biologically independent experiments. Results were compared using a two-way ANOVA followed by a Tukey's multi-comparisons test. *, P=0.0071; **, P=0.0434; ***, P=0.0026; ****, P=0.0021. **l**, Immunoblot detection of proteins from treated MEFs. Western blot images are representative of at least three biological replicates.

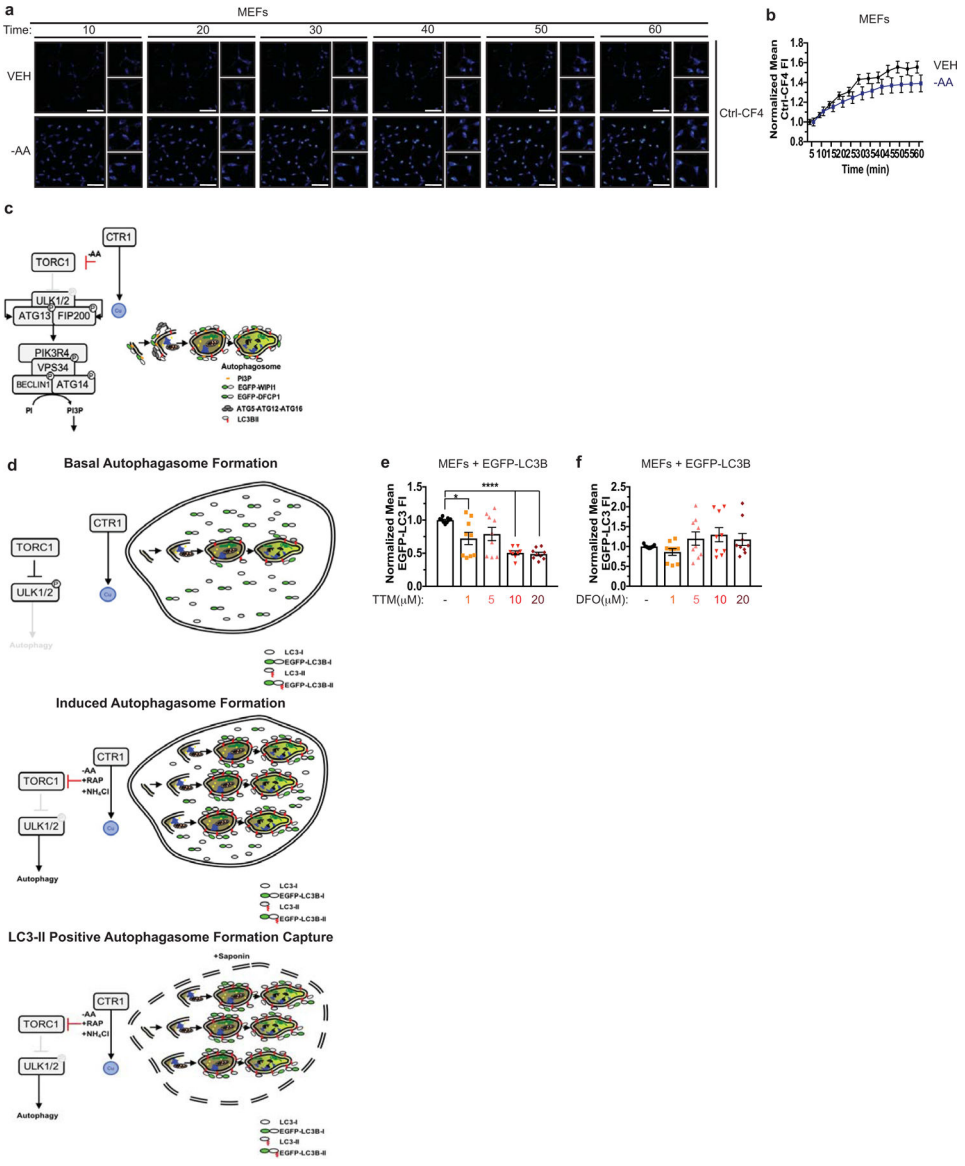

Extended Data 3. Cu but not Fe is required for autophagosome formation and is associated with fluctuations in the Cu labile pool.

a, Representative live cell imaging of the Cu probe Ctrl-CF4 every ten minutes for 60 minutes from MEFs treated with vehicle (VEH) or amino acid deprivation (-AA). Scale bar, 100 μm. **b**, Mean Ctrl-CF4 fluorescence intensity (FI) ± s.e.m. versus time (minutes, min) from MEFs treated with VEH or -AA normalized to t=0, five minutes. n=30 individual cells. Results were compared using a two-way ANOVA followed by a Sidak's multi-comparisons test. **c**, Schematic of immunofluorescence-based approach to access autophagosome formation. **d**, Schematic of flow cytometry-based approach to access autophagosome number. **e**,**f**, Scatter dot plot with bar at mean GFP-LC3 fluorescent intensity ± s.e.m. analyzed by flow cytometry from MEFs stably expressing *EGFP-LC3B* treated VEH or increasing concentrations of Cu chelator TTM (**e**) or Fe chelator DFO (**f**). n=9 biologically independent samples. Results were compared using a one-way ANOVA followed by a Dunnett's multi-comparisons test. *, P=0.0148; ****, P<0.0001.

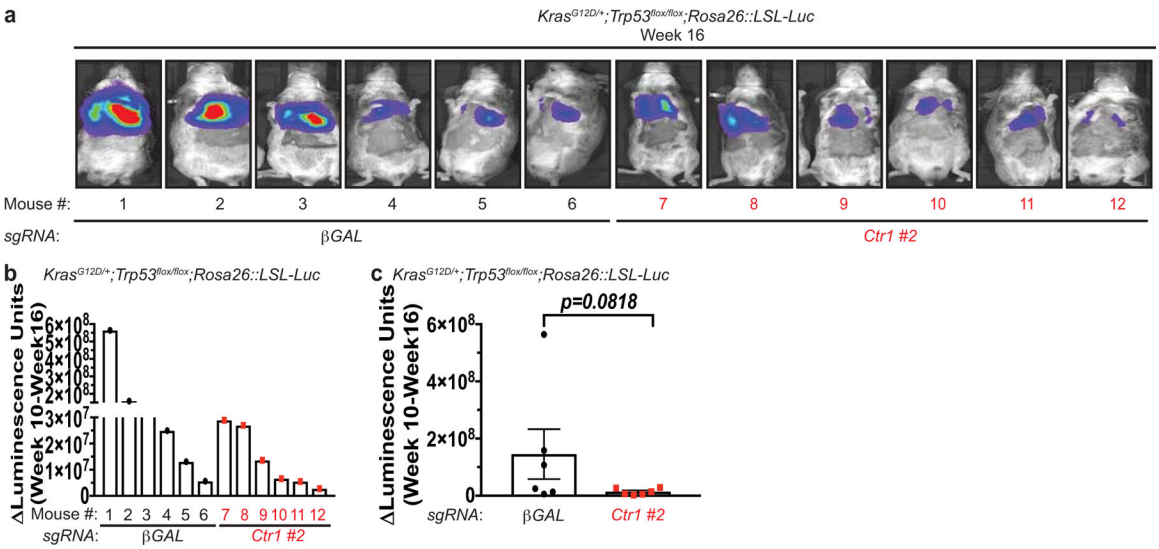

Extended Data 4. Genetic ablation of *Ctr1* reduces *Kras^{G12D}*-driven lung tumorigenesis.
a, Normalized representative images of *in vivo* luminescence of ***K**ras$^{G12D/+}$;Tr**p**53$^{flox/flox}$;Rosa26::LSL-**Luc*** (**KPLuc**) mice introduced with either *sgRNA* against *β-GAL* or *Ctr1* at week 16 endpoint. **b**,**c**, Scatter dot plot with bar at mean ΔLuminescence units from week 10 to week 16 from KPLuc mice introduced with either *sgRNA* against *β-GAL* or *Ctr1*. n=6 biologically independent animals. Results were compared using an unpaired, one-tailed Student's t-test. P=0.0818.

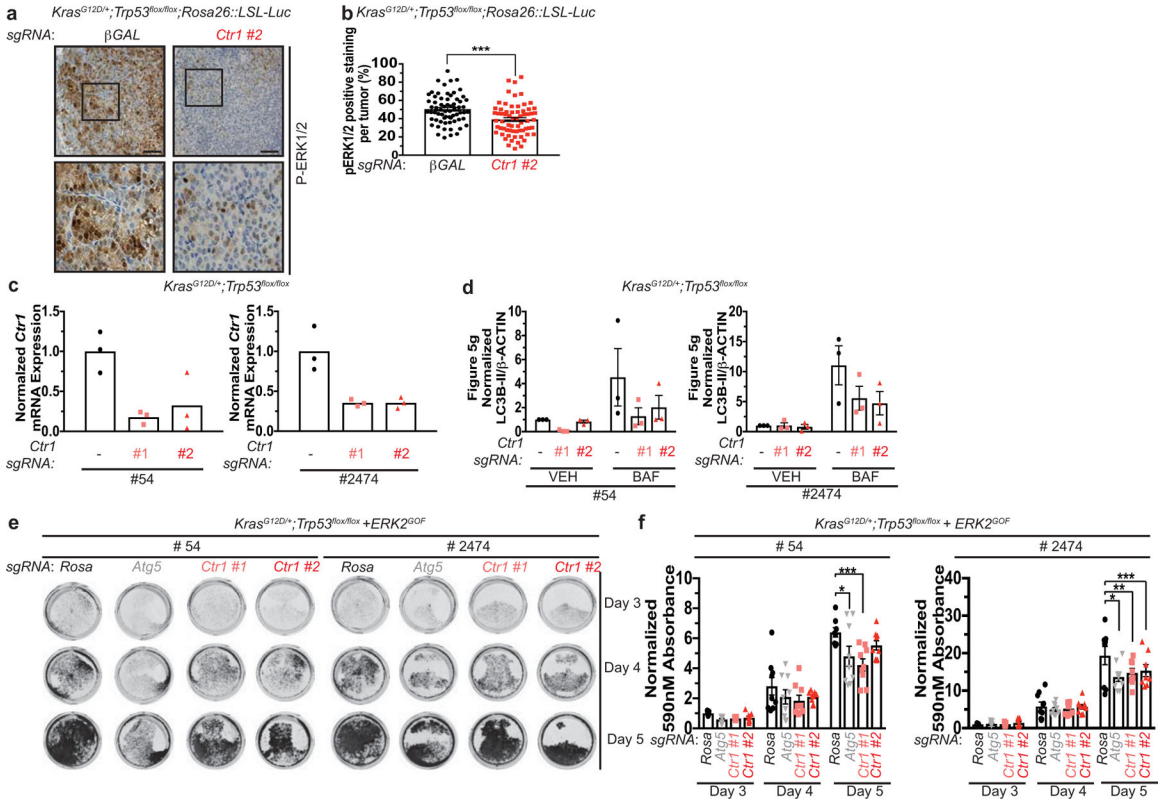

Extended Data 5. Genetic ablation of *Ctr1* decreases MAPK signaling to reduce *Kras*^{G12D}-driven lung tumorigenesis, while survival in response starvation is independent of MAPK signaling.

a, Representative 40x images of immunohistochemical detection of phosphorylated (P)-ERK1/2 of lungs from KPLuc mice expressing *sgRNA* against *β-GAL* or *Ctr1*. (40x scale bar: 50 μm). **b**, Scatter dot plot with bar at mean ± s.e.m. % P-ERK1/2 positive staining per tumor (*β-GAL* and *Ctr1*) from KPLuc mice expressing *sgRNA* against *β-GAL* or *Ctr1*. n=66 images. Results were compared using an unpaired, two-tailed Student's t-test. ***, P=0.0002. **c**, Scatter dot plot with bar at mean normalized quantitative PCR (qPCR) expression of *Ctr1* mRNA from KP lung adenocarcinoma cell lines #54 (KP #54) and #2474 (KP #2474) stably expressing *sgRNA* against *Rosa* (−) or *Ctr1* (*#1* or *#2*). n=1 performed in technical triplicate. **d**, Scatter dot plot with bar at mean normalized ΔLC3-II/β-ACTIN from Figure 5g. n=3 independent experiments. Results were compared using a two-way ANOVA followed by a Tukey's multi-comparisons test. ns. **e**, Representative crystal violet images of KP #54 and KP #2474 cells stably expressing *sgRNA* against *Rosa, Atg5,* or *Ctr1* (*#1* or *#2*) and ERK2^{GOF} from days 3, 4, and 5 of recovery. **f**, Scatter dot plot with bar at mean absorbance of extracted crystal violet at 590nM ± s.e.m. of KP #54 and KP #2474 cells stably expressing *sgRNA* against *Rosa, Atg5,* or *Ctr1* (*#1* or *#2*) and ***g***ain-***o***f-***f***unction (GOF) *HA-ERK2* (ERK2^{GOF}) from days 3, 4, and 5 of recovery normalized to *Rosa*, day 3 control. KP #54, n=# biologically independent samples; Day 3=9, Day 4=9, Day 5, *Rosa*=8, *Atg5*=9, *#1*=9, *#2*=9. *, P=0.0140; ***, P=0.0003. KP #2474, n=# biologically independent samples; Day 3=9, Day 4=9, Day 5, *Rosa*=9, *Atg5*=9, *#1*=8, *#2*=8. *, P=0.0011; **, P=0.0158; ***, P=0.0462.

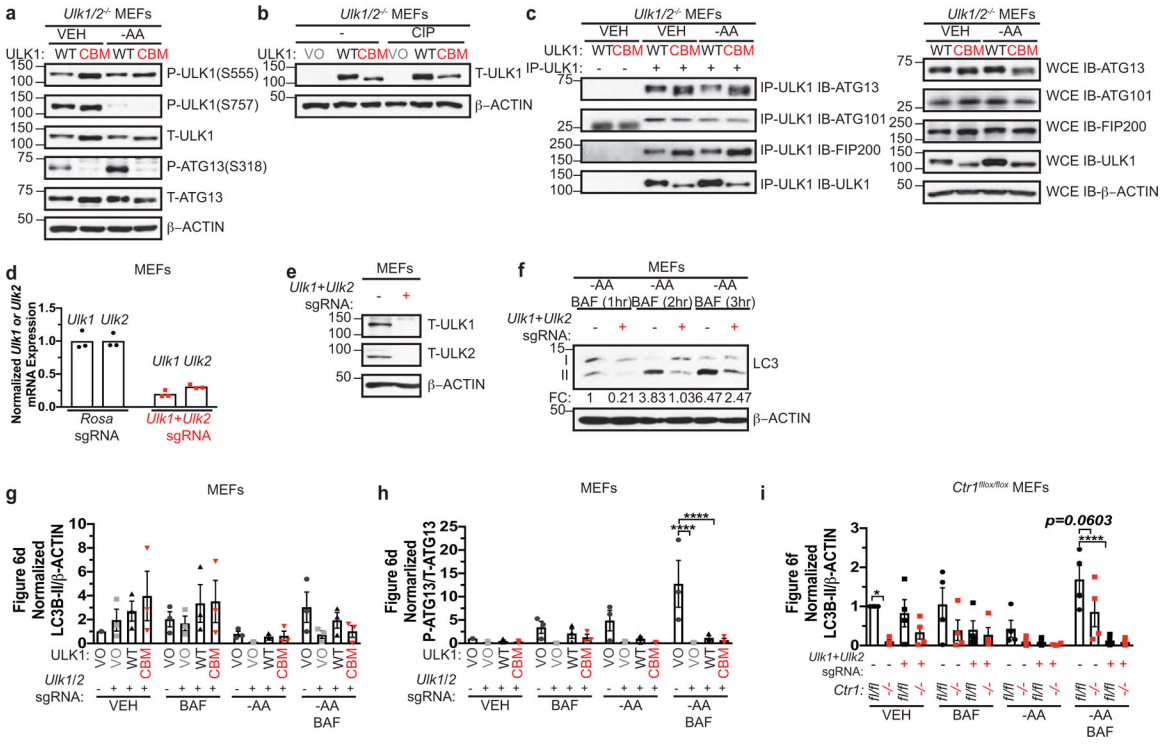

Extended Data 6. Binding of Cu to ULK1 is required for kinase activity but not substrate association or phosphorylation.

a, Immunoblot detection of phosphorylated (P) ATG13, total (T)- ATG13, P-ULK1 (S555), P-ULK1 (S757), T-ULK1, or β-ACTIN from *Ulk1/2*$^{-/-}$ MEFs stably expressing *HA-ULK1*^{WT} (WT) or *HA-ULK1*^{CBM} (CBM) treated with vehicle (VEH) or amino acid deprivation (-AA). **b**, Immunoblot detection of T-ULK1 or β-ACTIN from cell lysates treated with or without calf alkaline phosphatase (CIP) from *Ulk1/2*$^{-/-}$ MEFs stably expressing *empty vector* (VO), *HA-ULK1*^{WT} (WT), or *HA-ULK1*^{CBM} (CBM). **c**, Immunoblot detection of T-ATG13, T-ATG101, T-FIP200, T-ULK1, or β-ACTIN from immunoprecipitated (IP)-ULK1 or whole cell extracts (WCE) from *Ulk1/2*$^{-/-}$ MEFs stably expressing *HA-ULK1*^{WT} (WT) or *HA-ULK1*^{CBM} (CBM) treated with VEH or -AA. **d**, Scatter dot plot with bar at mean normalized quantitative PCR (qPCR) expression of *Ulk1* or *Ulk2* mRNA from MEFs stably expressing *sgRNA* against *Rosa* or *Ulk1* and *Ulk2*. n=1 performed in technical triplicate. **e**, Immunoblot detection of T-ULK1, T-ULK2, or β-ACTIN from MEFs stably expressing *sgRNA* against *Rosa* (−) or *Ulk1* and *Ulk2* (+). **f**, Immunoblot detection of LC3-I, LC3-II, or β-ACTIN from MEFs stably expressing *sgRNA* against *Rosa* (−) or *Ulk1* and *Ulk2* (+) treated with -AA and bafilomycin (BAF) for 1 hour (hr), 2 hr, and 3hr. **g**,**h**,**i**, Scatter dot plot with bar at mean normalized ΔLC3-II/β-ACTIN or ΔP-ATG13/T-ATG13 from Figure 6d,f. n=3 independent experiments. Results were compared using a two-way ANOVA followed by a Tukey's multi-comparisons test. **g**, ns; **h**, ****, P<0.0001. **i**, *, P=0.0365; ****, P<0.0001. Western blot images are representative of at least three biological replicates.

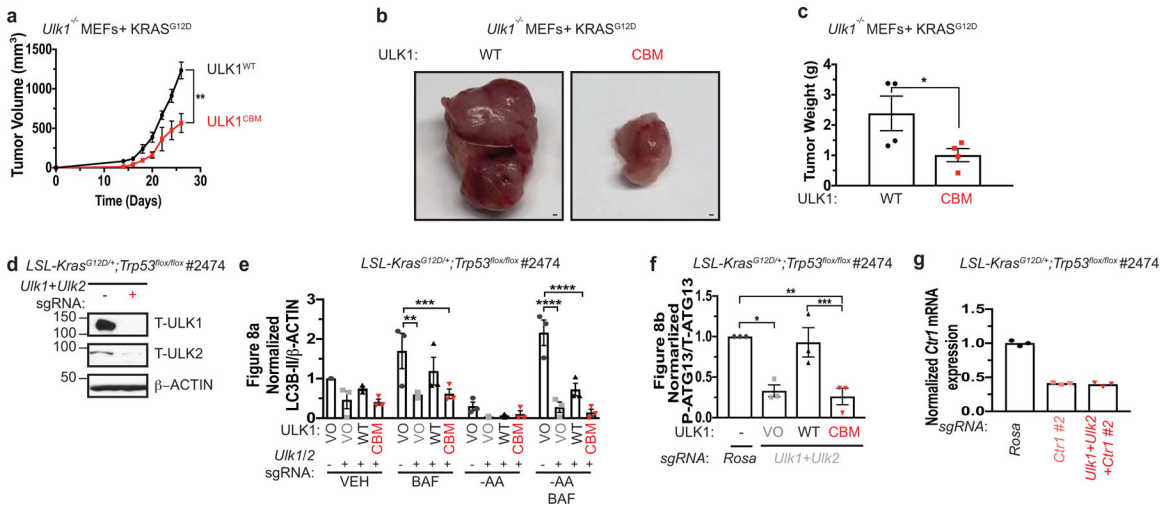

Extended Data 7. Binding of Cu to ULK1 is required for tumorigenesis by oncogenic KRAS^{G12D}.

a, Mean tumor volume (mm^3) ± s.e.m. versus time (days) in mice injected with *Ulk1*$^{-/-}$ MEFs stably expressing either *HA-ULK1*^{WT} or *HA-ULK1*^{CBM} and transformed with KRAS^{G12D}. n=4 biologically independent animals. Results were compared using a paired, one-tailed Student's t-test. **, P=0.0095. **b**, Representative dissected tumors from mice injected with *Ulk1*$^{-/-}$ MEFs stably expressing either *HA-ULK1*^{WT} (WT) or *HA-ULK1*^{CBM} (CBM) and transformed with KRAS^{G12D}. Scale bar, 100 μm. **c**, Scatter dot plot with bar at mean tumor weight (g) ± s.e.m. of tumors at endpoint from *Ulk1*$^{-/-}$ MEFs stably expressing either WT or CBM and transformed with KRAS^{G12D}. n=4 biologically independent samples. Results were compared using an unpaired, one-tailed Student's t-test. *, P=0.0325. n=4. **d**, Immunoblot detection of T-ULK1, T-ULK2, or β-ACTIN from ***Kras***$^{G12D/+}$;***Trp53***$^{flox/flox}$ (KP) lung adenocarcinoma cell line #2474 (KP #2474) stably expressing *sgRNA* against *Rosa* (−) or *Ulk1* and *Ulk2* (+). **e**,**f**, Scatter dot plot with bar at mean normalized ΔLC3-II/β-ACTIN or ΔP-ATG13/T-ATG13 from Figure 8a,b. n=3 independent experiments. Results were compared using a one-way ANOVA or a two-way ANOVA followed by a Tukey's multi-comparisons test. **e**, **, P=0.0013; ***, P=0.0016; ****, P<0.0001; **f**, *, P=0.0113; **, P=0.0063; ***, P=0.0113. **g**, Scatter dot plot with bar at mean normalized quantitative PCR (qPCR) expression of *Ctr1* mRNA from KP #2474 cells stably expressing *sgRNA* against *Rosa*, *Ctr1 #2*, or *Ulk1*, *Ulk2*, and *Ctr1 #2*. n=1 performed in technical triplicate.

Supplementary Material

Refer to Web version on PubMed Central for supplementary material.

Acknowledgements

We thank D.J. Thiele (Duke University), C.J. Chang (University of California Berkeley), R.K. Amaravadi (University of Pennsylvania), and S.A. Tooze (The Francis Crick Institute) for reagents and R.K. Amaravadi, I.A. Asangani, L. Busino, C.V. Dang, J.M. Davis, T.P. Gade, K.E. Hamilton, B. Keith, M.E. Murphy, R. Natesan, A.M. O'Reilly, S.W. Ryeom, M.C. Simon, B.Z. Stanger, J. Tobias, N.A. Tripp, A.T. Weerartna, K.E. Wellen, and E.S. Witze for technical support, discussions, and/or review of the manuscript. This work was supported by American Cancer Society Postdoctoral Fellowship 131203 PF 17 147 01 CCG (J.M.P), NIH grants GM124749 (D.C.B.),

CA193603 (D.M.F), CA222503 (D.M.F), ES019851 (M.C), CA243294 (T.T), Pew Scholars Program in Biomedical Science Award #50359 (D.C.B.), and V Foundation Scholar Award 3C59 8ABS 3424 3BDA (D.C.B).

References

1. Kolch W, Halasz M, Granovskaya M & Kholodenko BN The dynamic control of signal transduction networks in cancer cells. Nat. Rev. Cancer 15, 515–527 (2015). [PubMed: 26289315]
2. Festa RA & Thiele DJ Copper: an essential metal in biology. Curr. Biol 21, R877–83 (2011). [PubMed: 22075424]
3. Chelly J et al. Isolation of a candidate gene for Menkes disease that encodes a potential heavy metal binding protein. Nat. Genet 3, 14–19 (1993). [PubMed: 8490646]
4. Mercer JFB et al. Isolation of a partial candidate gene for Menkes disease by positional cloning. Nat. Genet 3, 20–25 (1993). [PubMed: 8490647]
5. Huster D et al. Consequences of copper accumulation in the livers of the Atp7b−/−(Wilson disease gene) knockout mice. Am. J. Pathol 168, 423–434 (2006). [PubMed: 16436657]
6. Pfeiffenberger J et al. Hepatobiliary malignancies in Wilson disease. Liver Int. 35, 1615–1622 (2015). [PubMed: 25369181]
7. Turski ML et al. A novel role for copper in Ras/MAPK signaling. Mol. Cell. Biol 32, 1284–1295 (2012). [PubMed: 22290441]
8. Brady DC et al. Copper is required for oncogenic BRAF signalling and tumorigenesis. Nature 509, 496–496 (2014).
9. Krishnamoorthy L et al. Copper regulates cyclic-AMP-dependent lipolysis. Nat. Chem. Biol 12, 586–592 (2016). [PubMed: 27272565]
10. Brady DC, Crowe MS, Greenberg DN & Counter CM Copper chelation inhibits BRAFV600E-driven melanomagenesis and counters resistance to BRAFV600E and MEK1/2 inhibitors. Cancer Res. 77, 6240–6252 (2017). [PubMed: 28986383]
11. Xu MM, Casio M, Range DE, Sosa JA & Counter CM Copper chelation as targeted therapy in a mouse model of oncogenic BRAF-driven papillary thyroid cancer. Clin. Cancer Res 24, 4271–4281 (2018). [PubMed: 30065097]
12. Goodman VL, Brewer GJ & Merajver SD Control of copper status for cancer therapy. Curr. Cancer Drug Targets 5, 543–549 (2005). [PubMed: 16305350]
13. Petherick KJ et al. Pharmacological inhibition of ULK1 kinase blocks mammalian target of rapamycin (mTOR)-dependent autophagy. J. Biol. Chem 290, 11376–11383 (2015). [PubMed: 25833948]
14. Chan EYW, Kir S & Tooze SA siRNA Screening of the Kinome Identifies ULK1 as a Multidomain Modulator of Autophagy. J Biol Chem 282, 25464–25474 (2007). [PubMed: 17595159]
15. Ganley IG et al. ULK1.ATG13.FIP200 complex mediates mTOR signaling and is essential for autophagy. J Biol Chem 284, 12297–12305 (2009). [PubMed: 19258318]
16. Hosokawa N et al. Nutrient-dependent mTORCl association with the ULK1-Atg13-FIP200 complex required for autophagy. Mol. Biol. Cell 20, 1981–1991 (2009). [PubMed: 19211835]
17. Jung CH et al. ULK-Atg13-FIP200 complexes mediate mTOR signaling to the autophagy machinery. Mol Biol Cell 20, 1992–2003 (2009). [PubMed: 19225151]
18. Kim D-H et al. mTOR Interacts with Raptor to Form a Nutrient-Sensitive Complex that Signals to the Cell Growth Machinery. Cell 110, 163–175 (2002). [PubMed: 12150925]
19. Thoreen CC et al. A unifying model for mTORC1-mediated regulation of mRNA translation. Nature 485, 109–113 (2012). [PubMed: 22552098]
20. Hara K et al. Amino Acid Sufficiency and mTOR Regulate p70 S6 Kinase and eIF-4E BP1 through a Common Effector Mechanism. J Biol Chem 273, 14484–14494 (1998). [PubMed: 9603962]
21. Kim E, Goraksha-Hicks P, Li L, Neufeld TP & Guan K-L Regulation of TORC1 by Rag GTPases in nutrient response. Nat Cell Biol 10, 935–945 (2008). [PubMed: 18604198]
22. Sancak Y et al. Ragulator-Rag complex targets mTORC1 to the lysosomal surface and is necessary for its activation by amino acids. Cell 141, 290–303 (2010). [PubMed: 20381137]

23. Inoki K, Zhu T & Guan K-L TSC2 Mediates Cellular Energy Response to Control Cell Growth and Survival. Cell 115, 577–590 (2003). [PubMed: 14651849]
24. Gwinn DM et al. AMPK phosphorylation of raptor mediates a metabolic checkpoint. Mol Cell 30, 214–226 (2008). [PubMed: 18439900]
25. Sabatini DM, Erdjument-Bromage H, Lui M, Tempst P & Snyder SH RAFT1: A mammalian protein that binds to FKBP12 in a rapamycin-dependent fashion and is homologous to yeast TORs. Cell 78, 35–43 (1994). [PubMed: 7518356]
26. Brown EJ et al. A mammalian protein targeted by G1-arresting rapamycin–receptor complex. Nature 369, 756–758 (1994). [PubMed: 8008069]
27. Brady GF et al. Regulation of the copper chaperone CCS by XIAP-mediated ubiquitination. Mol Cell Biol 30, 1923–1936 (2010). [PubMed: 20154138]
28. Xiao T et al. Copper regulates rest-activity cycles through the locus coeruleus-norepinephrine system. Nat. Chem. Biol 14, 655–663 (2018). [PubMed: 29867144]
29. Chiang GG & Abraham RT Phosphorylation of Mammalian Target of Rapamycin (mTOR) at Ser-2448 Is Mediated by p70S6 Kinase. J Biol Chem 280, 25485–25490 (2005). [PubMed: 15899889]
30. Brown EJ et al. Control of p70 s6 kinase by kinase activity of FRAP in vivo. Nature 377, 441–446 (1995). [PubMed: 7566123]
31. Soliman GA et al. mTOR Ser-2481 Autophosphorylation Monitors mTORC-specific Catalytic Activity and Clarifies Rapamycin Mechanism of Action. J Biol Chem 285, 7866–7879 (2010). [PubMed: 20022946]
32. Kim J, Kundu M, Viollet B & Guan K-L AMPK and mTOR regulate autophagy through direct phosphorylation of Ulk1. Nat Cell Biol 13, 132–141 (2011). [PubMed: 21258367]
33. Ichimura Y et al. A ubiquitin-like system mediates protein lipidation. Nature 408, 488–492 (2000). [PubMed: 11100732]
34. Gump JM et al. Autophagy variation within a cell population determines cell fate through selective degradation of Fap-1. Nat Cell Biol 16, 47–54 (2014). [PubMed: 24316673]
35. Pankiv S et al. p62/SQSTM1 binds directly to Atg8/LC3 to facilitate degradation of ubiquitinated protein aggregates by autophagy. J. Biol. Chem 282, 24131–24145 (2007). [PubMed: 17580304]
36. Itakura E & Mizushima N Characterization of autophagosome formation site by a hierarchical analysis of mammalian Atg proteins. Autophagy 6, 764–776 (2010). [PubMed: 20639694]
37. Mercer TJ, Gubas A & Tooze SA A molecular perspective of mammalian autophagosome biogenesis. J Biol Chem 293, 5386–5395 (2018). [PubMed: 29371398]
38. Karanasios E et al. Dynamic association of the ULK1 complex with omegasomes during autophagy induction. J Cell Sci 126, 5224–5238 (2013). [PubMed: 24013547]
39. Egan DF et al. Small Molecule Inhibition of the Autophagy Kinase ULK1 and Identification of ULK1 Substrates. Mol. Cell 59, 285–297 (2015). [PubMed: 26118643]
40. Russell RC et al. ULK1 induces autophagy by phosphorylating Beclin-1 and activating VPS34 lipid kinase. Nat Cell Biol 15, 741–750 (2013). [PubMed: 23685627]
41. Park YS et al. AKT-induced PKM2 phosphorylation signals for IGF-1-stimulated cancer cell growth. Oncotarget 7, 48155–48167 (2016). [PubMed: 27340866]
42. Dooley HC et al. WIPI2 links LC3 conjugation with PI3P, autophagosome formation, and pathogen clearance by recruiting Atg12-5-16L1. Mol Cell 55, 238–252 (2014). [PubMed: 24954904]
43. Eng KE, Panas MD, Hedestam GBK & McInerney GM A novel quantitative flow cytometry-based assay for autophagy. Autophagy 6, 634–641 (2010). [PubMed: 20458170]
44. Amaravadi RK, Kimmelman AC & Debnath J Targeting Autophagy in Cancer: Recent Advances and Future Directions. Cancer Discov. 9, 1167–1181 (2019). [PubMed: 31434711]
45. Strohecker AM et al. Autophagy Sustains Mitochondrial Glutamine Metabolism and Growth of BrafV600E–Driven Lung Tumors. Cancer Discov. 3, 1272–1285 (2013). [PubMed: 23965987]
46. Cancer Genome Atlas Research Network. Comprehensive molecular profiling of lung adenocarcinoma. Nature 511, 543–550 (2014). [PubMed: 25079552]
47. Guo JY et al. Autophagy suppresses progression of K-ras-induced lung tumors to oncocytomas and maintains lipid homeostasis. Genes Dev. 27, 1447–1461 (2013). [PubMed: 23824538]

48. Bryant KL et al. Combination of ERK and autophagy inhibition as a treatment approach for pancreatic cancer. Nat Med 25, 628–640 (2019). [PubMed: 30833752]

49. Kinsey CG et al. Protective autophagy elicited by RAF→MEK→ERK inhibition suggests a treatment strategy for RAS-driven cancers. Nat Med 25, 620–627 (2019). [PubMed: 30833748]

50. Lee C-S et al. MAP kinase and autophagy pathways cooperate to maintain RAS mutant cancer cell survival. Proc. Natl. Acad. Sci. U. S. A 116, 4508–4517 (2019). [PubMed: 30709910]

51. Guo JY et al. Autophagy provides metabolic substrates to maintain energy charge and nucleotide pools in Ras-driven lung cancer cells. Genes Dev. 30, 1704–1717 (2016). [PubMed: 27516533]

52. McAlpine F, Williamson LE, Tooze SA & Chan EYW Regulation of nutrient-sensitive autophagy by uncoordinated 51-like kinases 1 and 2. Autophagy 9, 361–373 (2013). [PubMed: 23291478]

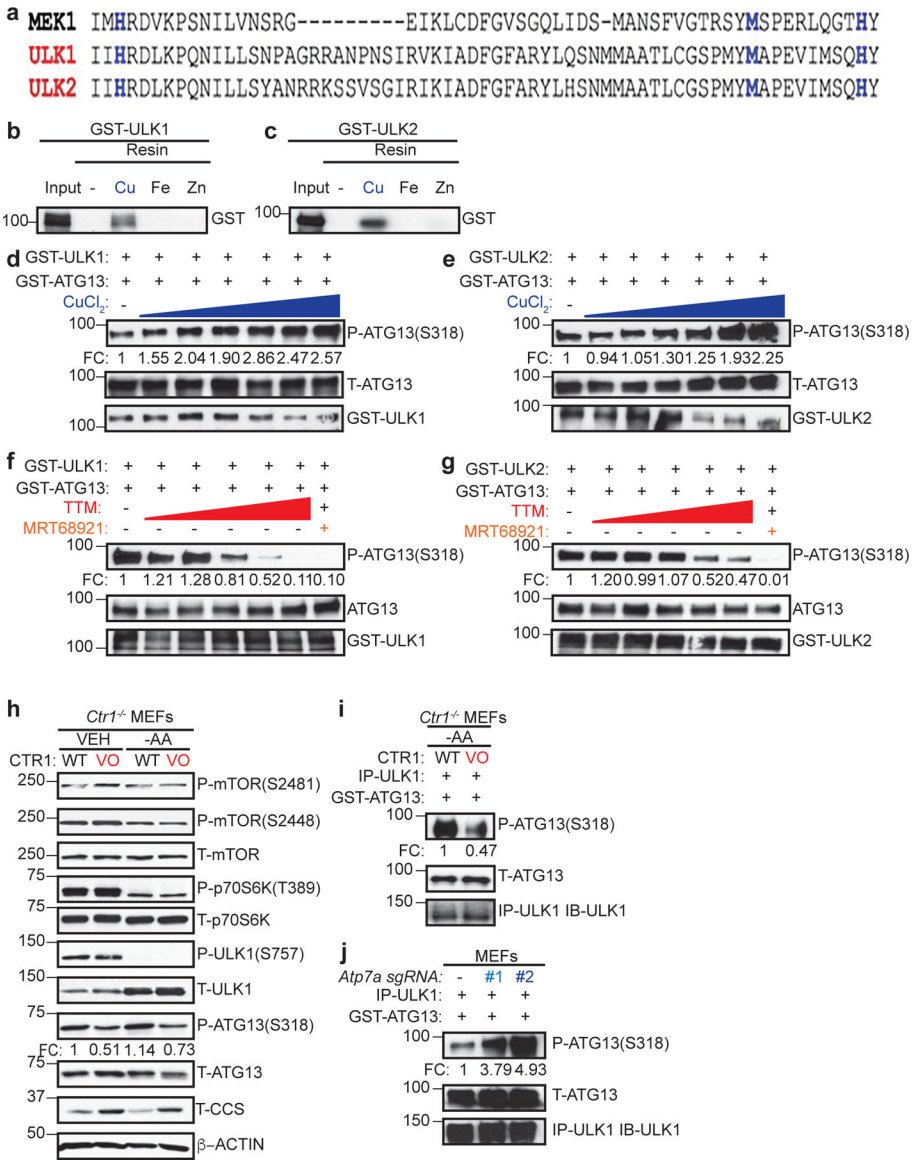

Figure 1. Cu binds to ULK1 and ULK2 and is required for kinase activity.

a, The amino-acid sequence of human MEK1 aligned to human ULK1 and human ULK2. Black letters, amino acids; blue letters, the four amino acids mutated in ***C***u-***b***inding ***m***utant (CBM) of MEK1 to decrease Cu binding and those conserved between ULK1 and ULK2. **b**,**c**, Immunoblot detection of recombinant GST-ULK1 or GST-ULK2 bound to a resin charged with or without Cu, Fe, or Zn compared to input. n=3 biologically independent experiments. **d**,**e**,**f**,**g**, Immunoblot detection of recombinant phosphorylated (P)-ATG13, total (T)-ATG13, and GST-ULK1 or GST-ULK2 from ULK1 or ULK2 *in vitro* kinase assays treated with or without increasing concentrations of $CuCl_2$ from 0 to 10 μM (**d**,**e**), with or without increasing concentrations of TTM from 0 to 50 μM, or 10 μM MRT68921 (**f**,**g**). Quantification: ΔP-ATG13/T-ATG13 normalized to GST-ULK1 and GST-ATG13 alone. **d**,**e**,**g**, n=3 biologically independent experiments. **g**, n=4 biologically independent experiments. **h**, Immunoblot detection of P- and/or T- mTOR, p70S6K, ULK1, ATG13,

CCS, or β-ACTIN from *Ctr1*$^{-/-}$ MEFs stably expressing *CTR1*^{WT} (WT) or *empty vector* (VO) treated with vehicle (VEH) or amino acid deprivation (-AA). Quantification: ΔP-ATG13/T-ATG13 normalized to WT, VEH control. n=3 biologically independent experiments. **i**,**j**, Immunoblot detection of recombinant P-ATG13, T-ATG13, or immunoprecipitated (IP)-ULK1 from immunocomplex ULK1 kinase assays from *Ctr1*$^{-/-}$ MEFs stably expressing WT or VO treated with VEH or -AA or MEFs stably expressing *sgRNA* against *Rosa* (−) or *Atp7a* (*#1* or *#2*). Quantification: ΔP-ATG13/T-ATG13 normalized to WT, VEH control or *Rosa* (−) control. n=3 biologically independent experiments.

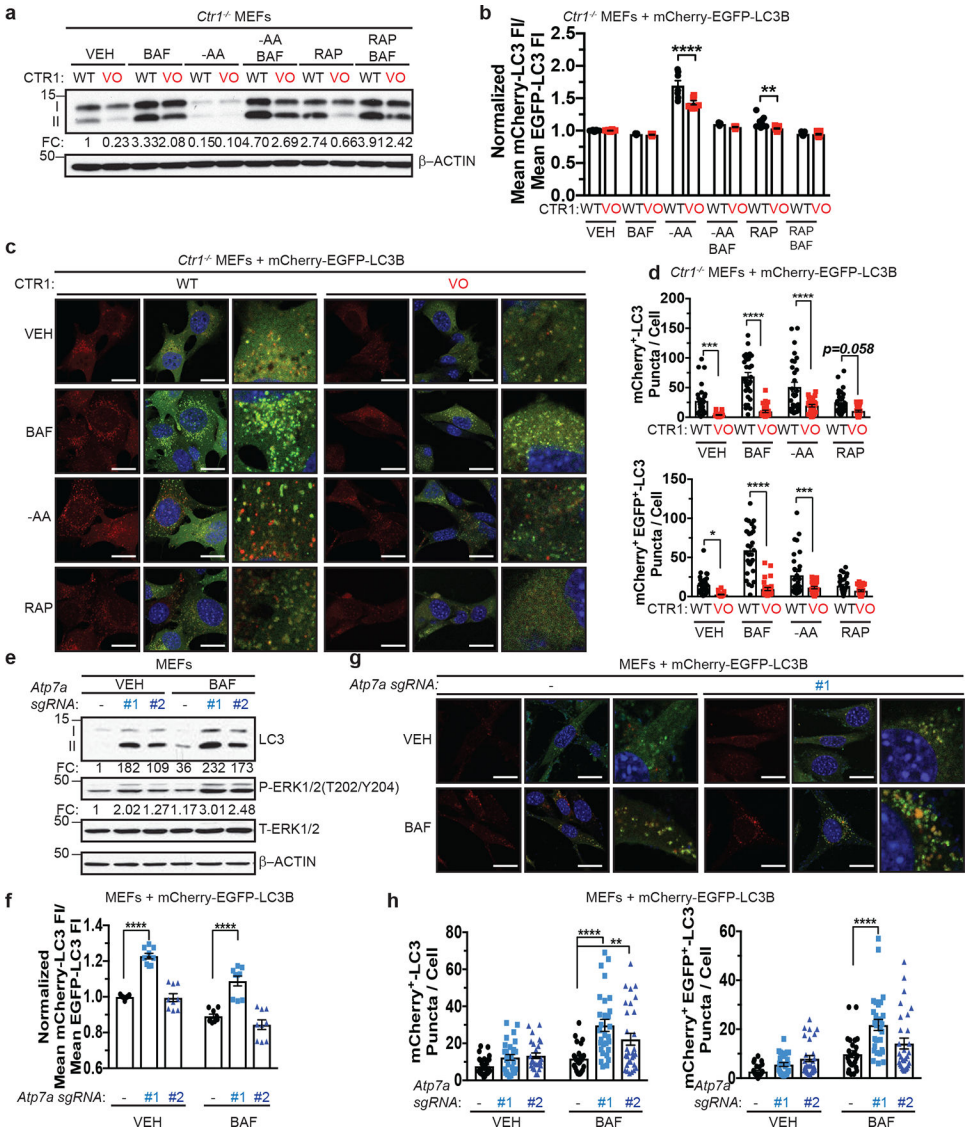

Figure 2. Genetic ablation or enhancement in intracellular Cu levels modulates autophagic flux.

a, Immunoblot detection of proteins from treated MEFs. Quantification: ΔLC3-II/β-ACTIN normalized to WT, VEH control. n=3 biologically independent experiments. **b**, Scatter dot plot with bar at mean mCherry-LC3 fluorescent intensity (FI)/mean EGFP-LC3 FI ± s.e.m. analyzed by flow cytometry from treated MEFs. N represents number[AU please clarify what the number is here.] of biologically independent samples, VEH n=16; BAF n=7; -AA n=7; -AA+BAF n=7; RAP, WT n=16, VO n=15; RAP+BAF n=13. Results were compared using a two-way ANOVA followed by a Sidak's multi-comparisons test. **, P=0.0035; ****, P<0.0001. **c**, Representative fluorescence images of EGFP, mCherry, or the merge from treated MEFs. Scale bar, 20 μm. **d**, Scatter dot plot with bar at mean mCherry^{+}-LC3 or mCherry^{+} EGFP^{+}-LC3 puncta per cell ± s.e.m. from treated MEFs. Results were compared using a two-way ANOVA followed by a Sidak's multi-comparisons test. n represents number of [AU please clarify the number which n represents] fields of view. Top, VEH n=30; BAF, WT n=30, VO n=29; -AA, WT n=30, VO n=28; RAP n=30; ***, P=0.0006;

****; P<0.001; Bottom, VEH, WT n=29, VO n=30; BAF, WT n=30, VO n=29; -AA, WT n=30, VO n=29; RAP, WT n=32, VO n=31; *, P=0.0147, ***; P=0.0009; ****, P<0.0001. **e**, Immunoblot detection of proteins from treated MEFs. Quantification: ΔLC3-II/T- β-ACTIN and ΔP-ERK1/2/T-ERK1/2 normalized to *Rosa* (−), VEH control. n=4 biologically independent experiments. **f**, Scatter dot plot with bar at mean mCherry-LC3 fluorescent intensity (FI)/mean EGFP-LC3 FI ± s.e.m. analyzed by flow cytometry from treated MEFs. n=9 biologically independent samples. Results were compared using a two-way ANOVA followed by a Sidak's multi-comparisons test. ****, P<0.0001. **g**, Representative fluorescence images of EGFP, mCherry, or the merge from treated MEFs. Scale bar, 20 μm. **h**, Scatter dot plot with bar at mean $mCherry^{+}$-LC3 or $mCherry^{+}$ $EGFP^{+}$-LC3 puncta per cell ± s.e.m. from treated MEFs. Results were compared using a two-way ANOVA followed by a Sidak's multi-comparisons test. n represents number of [AU please clarify this number] fields of view. Left, VEH, *Rosa n*=30, *#1 n*=29, *#2 n*=26, BAF, *Rosa n*=24, *#1 n*=29, *#2 n*=30; **, P=0.00911; ****, P<0.0001; Right, VEH, *Rosa n*=30, *#1 n*=27, *#2 n*=30; BAF, *Rosa n*=26, *#1 n*=29, *#2 n*=30; **, P=0.0042; ****, P<0.0001.

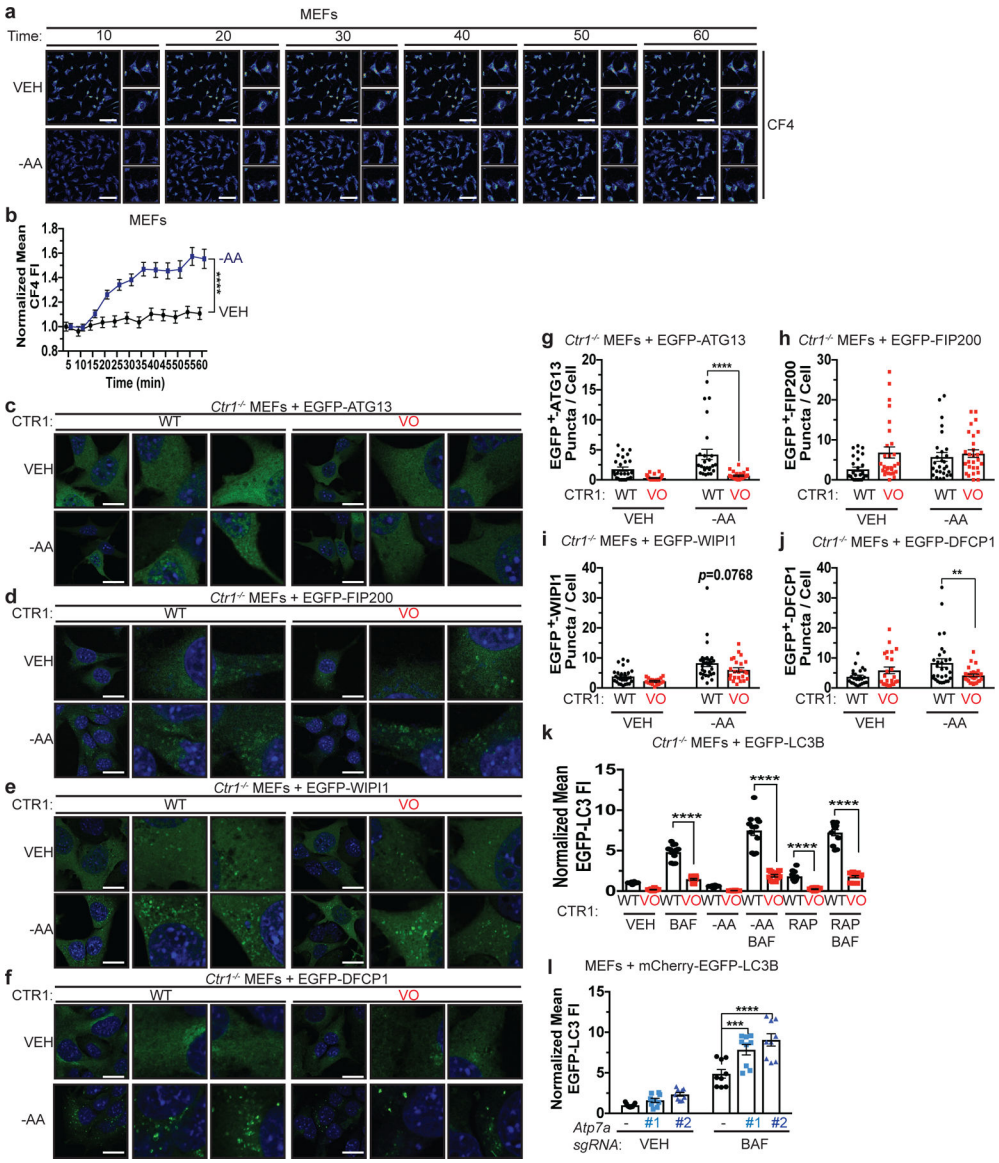

Figure 3. Cu is both necessary and sufficient for autophagosome formation.

a, Representative live cell imaging of the Cu probe CF4 every ten minutes for 60 minutes from MEFs treated with vehicle (VEH) or amino acid deprivation (-AA). Scale bar, 100 μm. **b**, Mean CF4 fluorescence intensity (FI) ± s.e.m. versus time (minutes, min) from MEFs treated with VEH or -AA normalized to t=0, five minutes. n=30 individual cells. Results were compared using a two-way ANOVA followed by a Sidak's multi-comparisons test. ****, P<0.0001. **c**,**d**,**e**,**f**, Representative fluorescence images of EGFP-ATG13 (**c**), EGFP-FIP200 (**d**), EGFP-WIP1 (**e**), or EGFP-DFCP1 (**f**) from *Ctr1*$^{-/-}$ MEFs stably expressing *CTR1*^{WT} (WT) or *empty vector* (VO) and *EGFP-ATG13*, *EGFP-FIP200*, *EGFP-WIP1*, or *EGFP-DFCP1* treated with VEH or -AA. Scale bar, 20 μm. **g**,**h**,**i**,**j**, Scatter dot plot with bar at mean EGFP^{+} puncta per cell ± s.e.m. from *Ctr1*$^{-/-}$ MEFs stably expressing WT or VO and *EGFP-ATG13* (**g**), *EGFP-FIP200* (**h**), *EGFP-WIP1* (**i**), or *EGFP-DFCP1* (**j**) treated with VEH or -AA. N represents number of[AU please clarify this number] fields of view. EGFP-

ATG13, VEH, WT n=27, VO n=26; -AA, WT n=26, VO n=27. EGFP-FIP200, VEH n=28; -AA, WT n=27, VO n=28. EGFP-WIP1, VEH, WT n=29, VO n=18; -AA, WT n=29, VO n=24. EGFP-DFCP1, VEH n=24, -AA n=29. Results were compared using a two-way ANOVA followed by a Sidak's multi-comparisons test. **, P=0.0057; ****, P<0.0001. **k**, Scatter dot plot with bar at mean EGFP-LC3 FI ± s.e.m. analyzed by flow cytometry from *Ctr1*$^{-/-}$ MEFs stably expressing WT or VO and *EGFP-LC3B* treated with VEH, -AA, or RAP with or without BAF normalized to WT, VEH control. Results were compared using a two-way ANOVA followed by a Sidak's multi-comparisons test. n=12 biologically independent samples. ****, P<0.0001. **l**, Scatter dot plot with bar at mean EGFP-LC3 FI ± s.e.m. analyzed by flow cytometry from MEFs stably expressing *sgRNA* against *Rosa* (−) or *Atp7a* (*#1* or *#2*) and *EGFP-LC3B* treated with VEH or BAF normalized to *Rosa* (−), VEH control. n=9 biologically independent samples. Results were compared using a two-way ANOVA followed by a Tukey's multi-comparisons test. ***, P=0.0002; ****, P<0.0001.

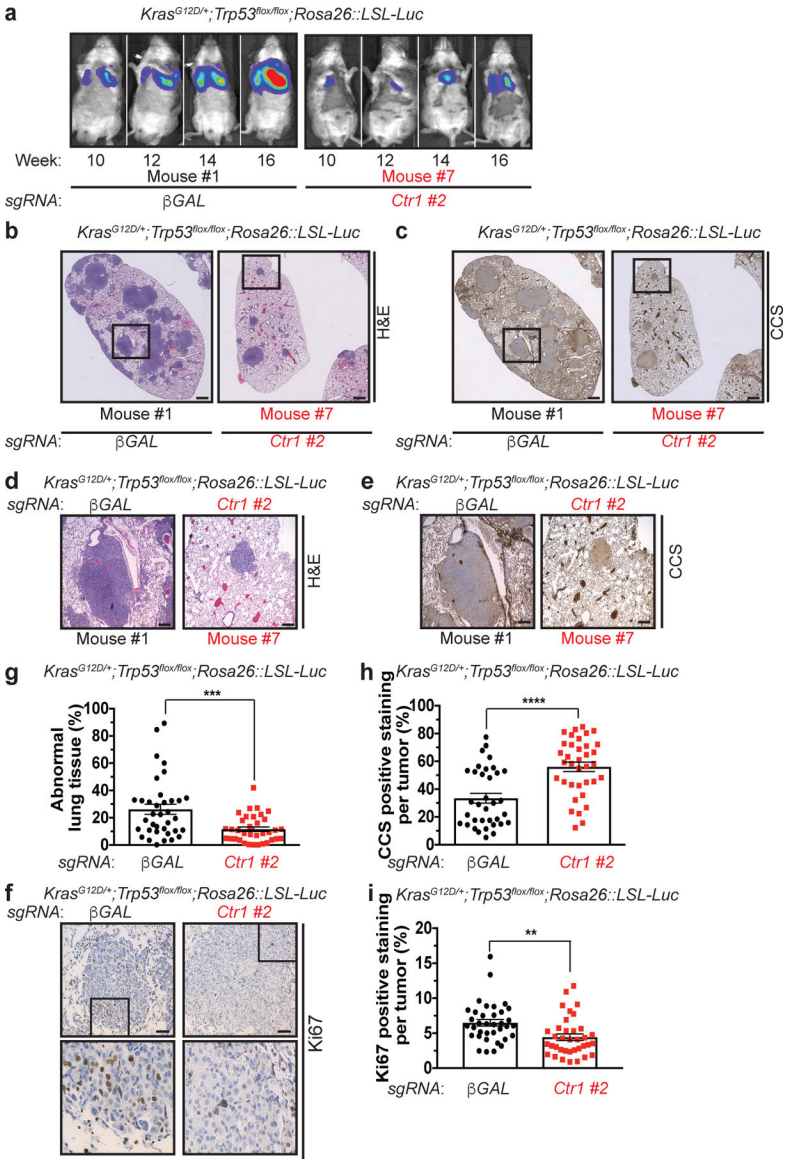

Figure 4. Genetic ablation of *Ctr1* decreases proliferation to reduce tumorigenesis in a mouse model of *Kras*^{G12D}-driven lung cancer.

a, Normalized representative images of *in vivo* luminescence of ***Kras***$^{G12D/+}$;***Tp53***$^{flox/flox}$;*Rosa26::LSL-**Luc*** (**KPLuc**) mice introduced with either *sgRNA* against *β-GAL* or *Ctr1* at indicated time points. n=6 biologically independent animals. **b**,**c**,**d**,**e**,**f**, Representative images of H&E stained (**b**,−5x stitched images, **d**-5x); immunohistochemical detection of CCS (**c**-5x stitched images, **e**-5x), or Ki67 (**f**-40x) of lungs from KPLuc mice expressing *sgRNA* against *β-GAL* or *Ctr1* (5x stitched scale bar: 250 μm; 5x scale bar: 250 μm; 40x scale bar: 50 μm). **g**,**h**,**i**, Scatter dot plot with bar at mean ± s.e.m. % abnormal lung tissue (**g**, *β-GAL*, n=36 images; *Ctr1*, n=35 images), % CCS positive staining per tumor (**h**, *β-GAL*, n=35 images; *Ctr1*, n=36 images), or % Ki67 positive staining per tumor (**i**, n=36 images) from KPLuc mice expressing *sgRNA* against *β-GAL* or *Ctr1*. Results were compared using an unpaired, one-tailed Student's t-test. **, P=0.0025; ***, P=0.0006; ****, P<0.0001.

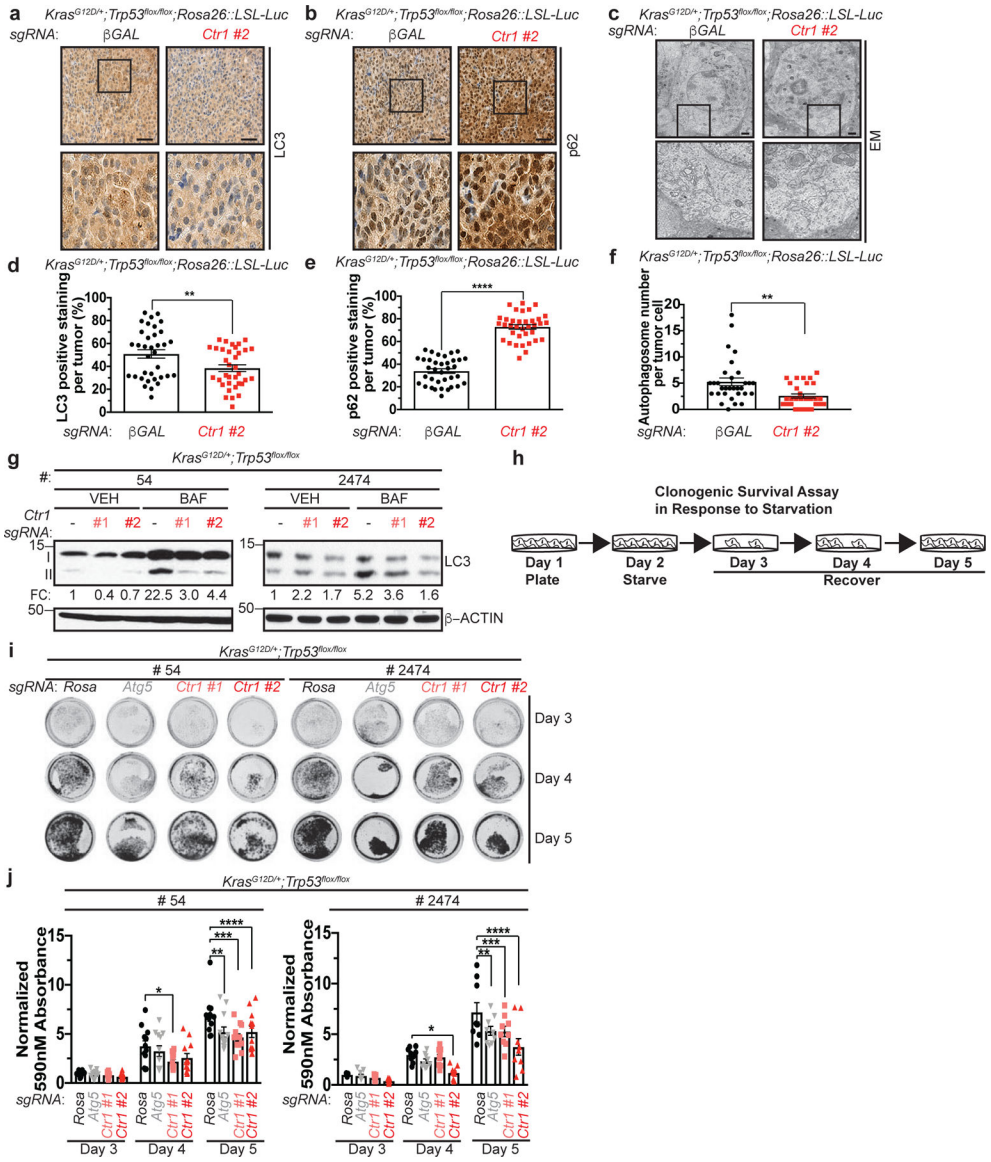

Figure 5. Genetic ablation of *Ctr1* decreases autophagy to reduce tumorigenesis and sensitizes cancer cells to starvation in a mouse model of *Kras*^{G12D}-driven lung cancer.

a,**b**,**c**, Representative images of immunohistochemical detection of LC3 (**a**-40x) or p62 (**b**-40x); or electron microscopy (EM) (**c**) of lungs from KPLuc mice expressing *sgRNA* against *β-GAL* or *Ctr1* (40x scale bar: 50 μm; EM scale bar: 1 μm). **d**,**e**,**f**, Scatter dot plot of mean ± s.e.m. % LC3 positive staining per tumor (**d**, n=35 images), % p62 positive staining per tumor (**e**, n=35 images), or autophagosome number per tumor cell (**f**, *β-GAL*, n=31 images; *Ctr1*, n=30 images) from KPLuc mice expressing *sgRNA* against *β-GAL* or *Ctr1*. Results were compared using an unpaired, one-tailed Student's t-test. **d**, **, P=0.0098; **e**, ****, P<0.0001; **f**, **, P=0.0024. **g**, Immunoblot detection of LC3-I, LC3-II, or β-ACTIN from KP lung adenocarcinoma cell lines #54 (KP #54) and #2474 (KP #2474) stably expressing *sgRNA* against *Rosa* (−) or *Ctr1* (*#1* or *#2*) treated with vehicle (VEH) or bafilomycin (BAF). Quantification: ΔLC3-II/β-ACTIN normalized to *Rosa* (−), VEH control. n=3 biologically independent experiments. **h**, Schematic of clonogenic survival

assay in response to starvation. KP #54 and KP #2474 cells stably expressing *sgRNA* against *Rosa, Atg5*, or *Ctr1* following one day of starvation (EBSS) were recovered for three days in normal medium (DMEM). **i**, Representative crystal violet images of KP #54 and KP #2474 cells stably expressing *sgRNA* against *Rosa, Atg5*, or *Ctr1* (*#1* or *#2*) from days 3, 4, and 5 of recovery. **j**, Scatter dot plot with bar at mean absorbance of extracted crystal violet at 590nM ± s.e.m. of KP #54 and KP #2474 cells stably expressing *sgRNA* against *Rosa*, *Atg5*, or *Ctr1* (*#1* or *#2*) from days 3, 4, and 5 of recovery normalized to *Rosa*, day 3 control. Results were compared using a two-way ANOVA followed by a Tukey's multi-comparisons test. KP #54, n represents number of biologically independent samples; Day 3 n=12, Day 4 n=12, Day 5, *Rosa n*=11, *Atg5 n*=12, *#1 n*=12, *#2 n*=12. *, P=0.0344; **, P=0.0209; ***, P=0.0010; ****, P=0.0229. KP #2474, n=9 biologically independent samples; *, P=0.0228; **, P=0.0191; ***, P=0.0148; ****, P<0.0001.

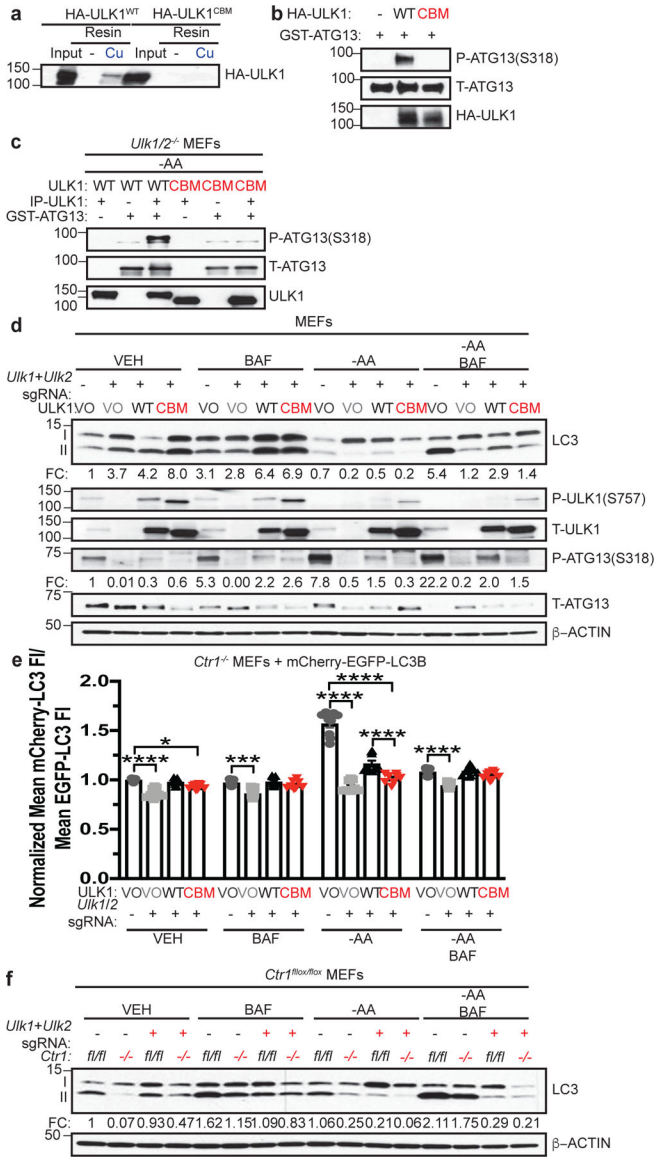

Figure 6. Binding of Cu to ULK1 is required for autophagy signaling and induction.

a, Immunoblot detection of recombinant HA-ULK1^{WT} or ***C***u ***b***inding ***m***utant HA-ULK1^{CBM} bound to a resin charged with or without Cu compared to input. n=3 biologically independent experiments. **b**, Immunoblot detection of recombinant phosphorylated (P)-ATG13, total (T)-ATG13, and HA-ULK1^{WT} or HA-ULK1^{CBM} from ULK1 *in vitro* kinase assays. n=3 biologically independent experiments. **c**, Immunoblot detection of recombinant P-ATG13, T-ATG13, or immunoprecipitated (IP)-ULK1 from *Ulk1/2*$^{-/-}$ MEFs stably expressing *HA-ULK1*^{WT} (WT) or *HA-ULK1*^{CBM} (CBM) treated with amino acid deprivation (-AA). n=3 biologically independent experiments. **d**, Immunoblot detection of LC3-I, LC3-II, P-ULK1, T-ULK1, P-ATG13, T-ATG13, or β-ACTIN from MEFs stably expressing *sgRNA* against *Rosa* (−) reconstituted with *empty vector* (VO) or *sgRNA* against *Ulk1* and *Ulk2* reconstituted with *empty vector* (VO), *HA-ULK1*^{WT} (WT), or *HA-ULK1*^{CBM} (CBM) treated with vehicle (VEH) or -AA with or without bafilomycin (BAF).

Quantification: ΔLC3-II/β-ACTIN and ΔP-ATG13/T-ATG13 normalized to *Rosa* (−), VO, VEH control. n=3 biologically independent experiments. **e**, Scatter dot plot with bar at mean mCherry-LC3 fluorescent intensity (FI)/mean EGFP-LC3 FI ± s.e.m. analyzed by flow cytometry from MEFs stably expressing *sgRNA* against *Rosa* (−) reconstituted with VO or *sgRNA* against *Ulk1* and *Ulk2* reconstituted with VO, WT, or CBM and *mCherry-EGFP-LC3B* treated with VEH or -AA with or without BAF normalized to *Rosa* (−), VO, VEH control. n= number of biologically independent samples; VO=9, VO=9, WT=9, CBM=8. Results were compared using a two-way ANOVA followed by a Tukey's multi-comparisons test. *, P=0.0335; ***, P=0.0002; ****, P<0.0001. **f**, Immunoblot detection of LC3-I, LC3-II, or β-ACTIN from $Ctr1^{flox/flox}$ (*fl/fl*) or $Ctr1^{-/-}$ (−/−) MEFs stably expressing *sgRNA* against *Rosa* (−) or *sgRNA* against *Ulk1* and *Ulk2* (+) treated with VEH or -AA with or without BAF. Quantification: ΔLC3-II/β-ACTIN normalized to $Ctr1^{flox/flox}$, *Rosa* (−), VEH control. n=4 biologically independent experiments.

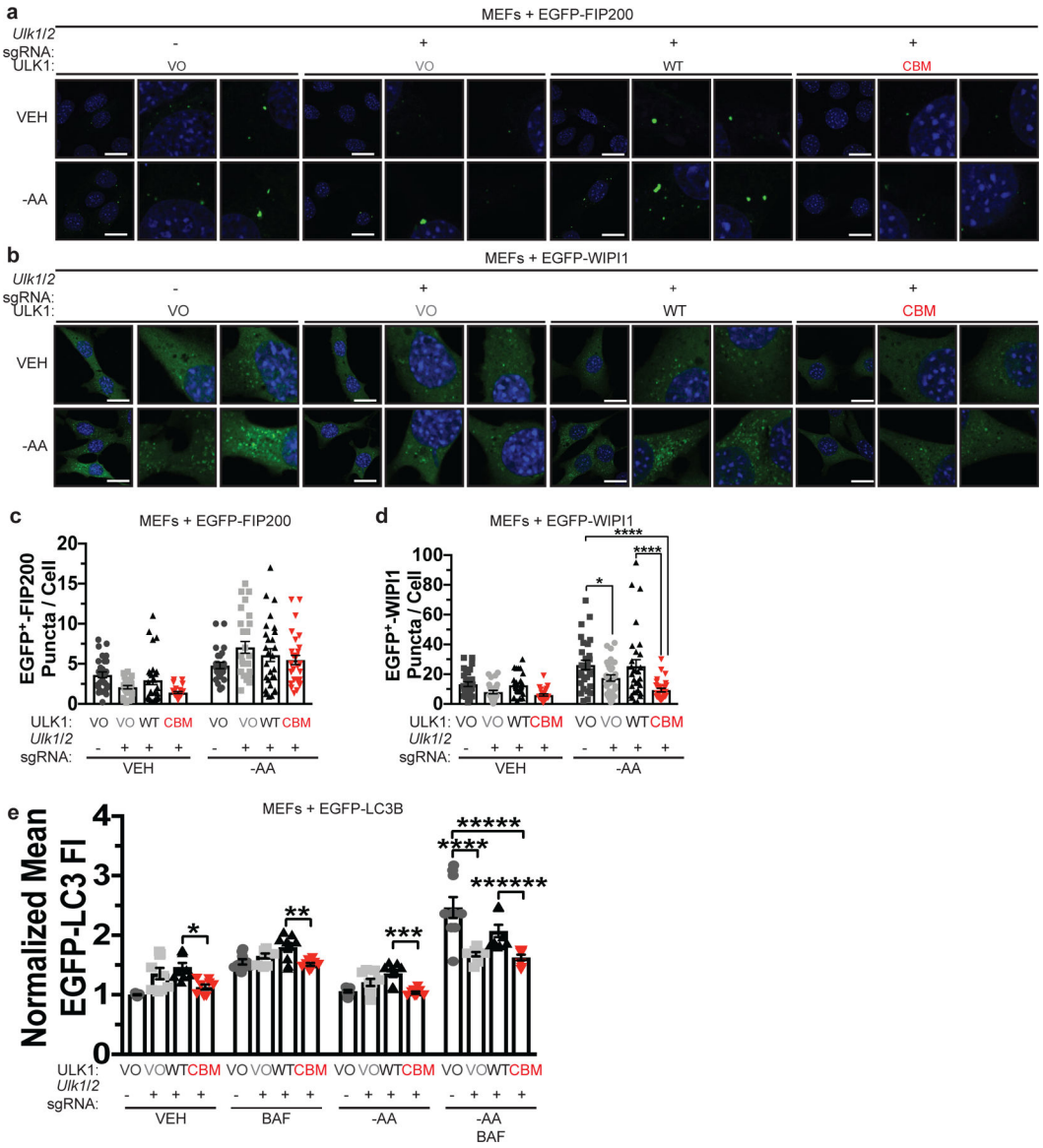

Figure 7. Binding of Cu to ULK1 is required for autophagosome complex formation.

a,**b**, Representative fluorescence images of EGFP-FIP200 (**a**) or EGFP-WIP1 (**b**) from MEFs stably expressing *sgRNA* against *Rosa* (−) reconstituted with VO or *sgRNA* against *Ulk1* and *Ulk2* reconstituted with VO, WT, or CBM and *EGFP-FIP200* or *EGFP-WIP1* treated with VEH or -AA. Scale bar, 20 μm. **c**,**d**, Scatter dot plot with bar at mean mean EGFP^{+} puncta per cell ± s.e.m. from MEFs stably expressing *sgRNA* against *Rosa* (−) reconstituted with VO or *sgRNA* against *Ulk1* and *Ulk2* reconstituted with VO, WT, or CBM and *EGFP-FIP200* (**c**) or *EGFP-WIP1* (**d**) treated with VEH or -AA. n represents number offields of view. EGFP-FIP200, VEH, VO=30, VO=27, WT=28, CBM=27; -AA, VO=26, VO=28, WT=28, CBM=29; EGFP-WIP1, VEH, VO=30, VO=28, WT=30, CBM=28; -AA, VO=29, VO=30, WT=29, CBM=30. Results were compared using a two-way ANOVA followed by a Sidak's multi-comparisons test. *, P=0.0394; ****, P<0.0001. **e**, Scatter dot plot with bar at mean EGFP-LC3 FI ± s.e.m. analyzed by flow cytometry from

MEFs stably expressing *sgRNA* against *Rosa* (−) reconstituted with VO or *sgRNA* against *Ulk1* and *Ulk2* reconstituted with VO, WT, or CBM and *EGFP-LC3B* treated with VEH or -AA with or without BAF normalized to *Rosa* (−), VO, VEH control. N represents number of biologically independent samples. VO=9, VO=9, WT=9, CBM=8. Results were compared using a two-way ANOVA followed by a Sidak's multi-comparisons test. *, P=0.0083; **, P=0.0321; ***, P=0.0125; ****, P<0.0001; *****, P<0.0001; ******, P=0.0002.

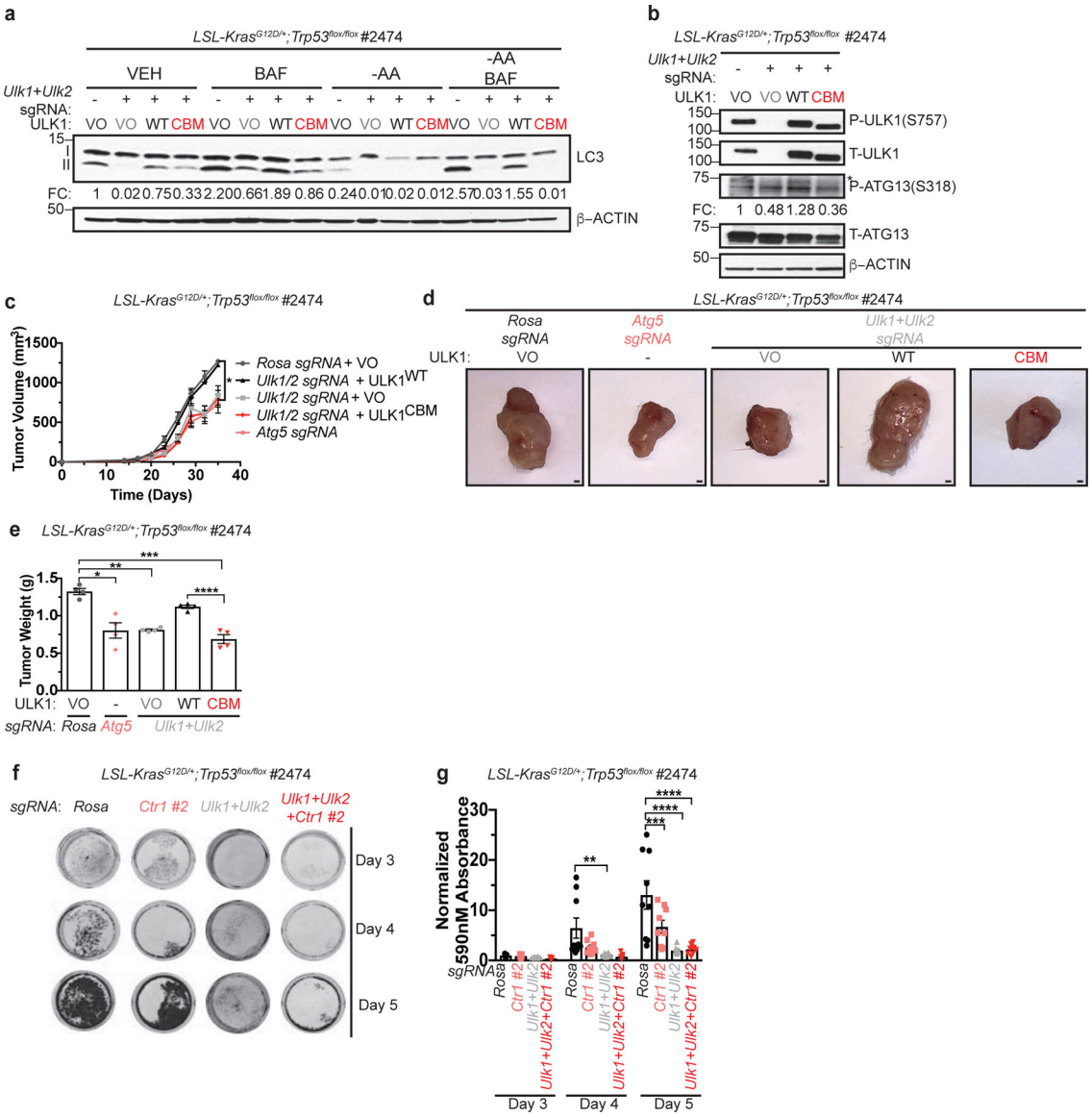

Figure 8. Binding of Cu to ULK1 is required for KRAS^{G12D}-driven tumor growth and cancer cell survival in response to starvation.

a, Immunoblot detection of proteins from treated KP cells. Quantification: ΔLC3-II/β-ACTIN normalized to *Rosa* (−), VO, VEH control. n=3 biologically independent experiments. **b**, Immunoblot detection of proteins from treated KP cells. Quantification: ΔP-ATG13/T-ATG13 normalized to *Rosa* (−), VO, VEH control. n=3 biologically independent experiments. **c**, Mean tumor volume (mm^3) ± s.e.m. versus time (days) in mice injected with KP cells. n=4 biologically independent animals. Results were compared using a paired, two-tailed Student's t-test. *Rosa* vs. *Atg5*, *, P=0.0228; *Rosa* vs. *Ulk1/2*, *, P=0.0176; *Ulk1/2* vs. *Ulk1/2* + ULK1^{WT}, *, P=0.0199; *Rosa* vs. *Ulk1/2* + ULK1^{CBM}, *, P=0.0116; *Ulk1/2* + ULK1^{WT} vs. *Ulk1/2* + ULK1^{CBM}, *, P=0.0157. **d**, Representative dissected tumors from mice injected with KP cells. Scale bar, 100 μm. **e**, Scatter dot plot with bar at mean tumor weight (g) ± s.e.m. of KP tumors at endpoint. n=4 biologically independent animals. Results were compared using a two-way ANOVA followed by a Tukey's multi-comparisons test. *,

P=0.0001; **, P=0.0001; ***, P<0.0001; ****, P=0.0007. **f**, Representative crystal violet images of KP cells from days 3, 4, and 5 of recovery. **g**, Scatter dot plot with bar at mean absorbance of extracted crystal violet at 590nM ± s.e.m. of KP cells from days 3, 4, and 5 of recovery normalized to *Rosa*, day 3 control. N represents number of biologically independent samples. *Rosa*=9, *Ctr1 #2 n*=9, *Ulk1/2 n*=12, *Ctr1 #2 + Ulk1/2 n*=9. Results were compared using a two-way ANOVA followed by a Tukey's multi-comparisons test. **, P=0.0010; ***, P=0.0002; ****, P<0.0001.